AD-A115 388 FOREIGN TECHNOLOGY DIV WRIGHT-PATTERSON AFB OH F/G 20/4
ACTA MECHANICA SINICA (SELECTED ARTICLES).(U)
MAY 82
UNCLASSIFIED FTD-ID(RS)T-1759-81 NL

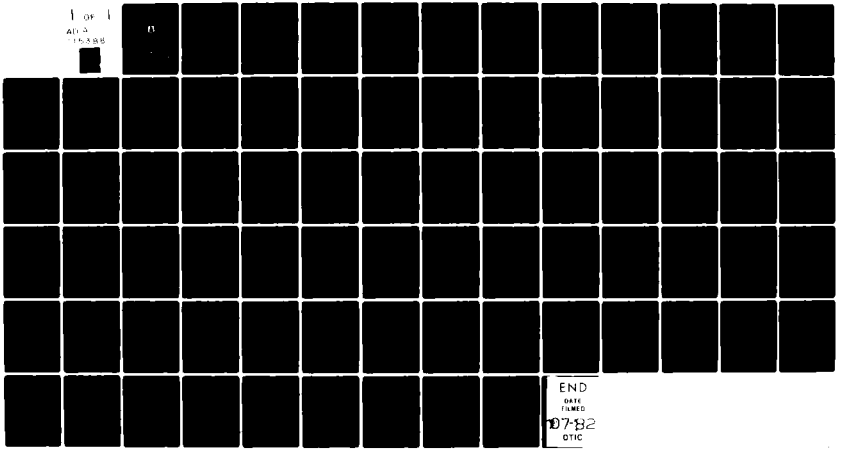

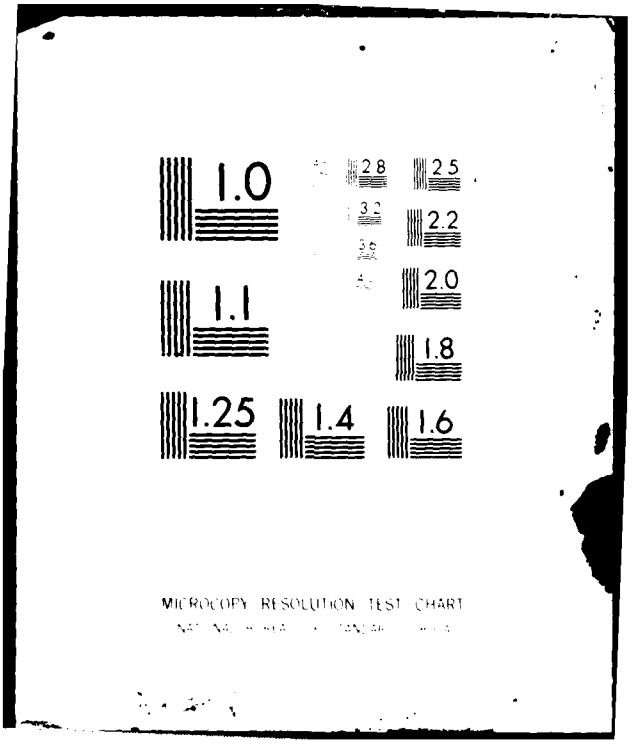
1.0
2.8
2.5
3.2
2.2
3.6
4.0
2.0
1.1
1.8
1.25
1.4
1.6
MICROCOPY RESOLUTION TEST CHART

FTD-ID(RS)T-1759-81

FOREIGN TECHNOLOGY DIVISION

ACTA MECHANICA SINICA

(Selected Articles)

Approved for public release;
distribution unlimited.

EDITED TRANSLATION

FTD-ID(RS)T-1759-81 4 May 1982

MICROFICHE NR: FTD-82-C-000587

ACTA MECHANICA SINICA (Selected Articles)

English pages: 70

Source: Acta Mechanica Sinica, Nr. 5, 1981,
pp. 421-438; 445-451; 507-510; 516-520

Country of origin: China
Translated by: LEO KANNER ASSOCIATES
F33657-81-D-0264
Requester: FTD/TQTA

PREPARED BY:

TRANSLATION DIVISION
FOREIGN TECHNOLOGY DIVISION
WP-AFB, OHIO.

Table of Contents

Variational Principles and Generalized Principle for Three-Dimensional Transonic Flow with Shock Waves in a Rotating Turbo-Impeller, by Liu Gaolian 1

Calculation for Three-Dimensional Turbulent Boundary Layer on a Yawed Wing in Compressible Flow, by Zhang Guofu 19

On the Rayleigh-Taylor Instability of a Current Sheet in an Electromagnetically Driven Shock Wave Apparatus, by Xu Fu 39

Measurement of Electron Density Behind a Strong Shock Wave Using 3 cm Microwave Transmission, by Zhu Naiyi and Li Xuefen 51

The Interference Factor of Vortex Lift of Wing-Body Combinations at Supersonic Speed, by Yin Xieyuan 60

GRAPHICS DISCLAIMER

All figures, graphics, tables, equations, etc. merged into this translation were extracted from the best quality copy available.

VARIATIONAL PRINCIPLES AND GENERALIZED PRINCIPLE FOR THREE-DIMENSIONAL TRANSONIC FLOW WITH SHOCK WAVES IN A ROTATING TURBO-IMPELLER

by Liu Gaolian
(Shanghai Institute of Mechanical Engineering)

Abstract

In this article a family of variational principles for three-dimensional transonic steady relative flow with embedded shocks in a turbomachine impeller of axial radial or mixed flow type is developed. Its special feature is to take full advantage of natural boundary conditions and "artificial interfaces," and besides converting all boundary conditions into natural ones, it is also shown that by taking variations of the position of unknown flow discontinuities (such as shocks and free trailing vortex sheets), all matching conditions across these discontinuities, including the well-known Rankine-Hugoniot shock relations, can be derived from the variational principles as natural interface conditions.

This article is primarily intended to provide, in conjunction with the discontinuous finite element, a theoretical basis for developing a new computational method which allows all flow discontinuities (including the shock surface and free trailing vortex sheets) to be singled out automatically and distinctly. Owing to the use of a potential function, the results in this article are limited to cases where the Mach numbers before the shock do not differ greatly from one.

In the appendix, an analogy between the functional variations with variable domain and the Reynold's transport theorem is pointed out and used as a basis for deriving a general formula for such variations.

1. Preface

Following the continuous development of high voltage, high speed, high temperature and high efficiency impellers, transonic flows increasingly appeared. Owing to the simultaneous existence of the subsonic and supersonic areas, the flow field's physical properties (domain of dependence and domain of influence) and mathematical properties (elliptic type and hyperbolic) are all very different. When the shape of its interface is unknown, especially the discontinuities which have yet to appear, the problem of deriving the transonic flow field is difficult yet is of real significance.

At present, the two major methods for deriving the transonic flow field are the non-steady variation method [3] and relaxation method. Although both methods are automatic, yet neither can distinctly compute (widened to a difference network) the discontinuities. Moreover, the computation time for the non-steady variation method is very long and it is also difficult to apply. On the other hand, although the shock fitting method is able to be distinct, yet it is still unable to compute the discontinuities automatically. Therefore, it is very difficult to apply to the problem of the complex internal flow of the shock system. The variational principles can also be taken as the basis for deriving the transonic flow (for example, references [9-11]), yet all are limited by the planar wing, especially the problem of not taking into consideration the handling of various unknown discontinuities. Because reference [10] takes the positions of the shock as

known, theoretically it is incomplete and unsuitable for application.

In the last several years, the three-dimensional aerodynamic theory for impellers has advanced rapidly in the area of positive propositions. Aside from using the quasi-three-dimensional theory which is based on the two relative flow theories mentioned in reference [1], there has been great effort expended both domestically and abroad to find a general theory and method for deriving three-dimensional flow (for example, references [2-4]).

This article, on the basis of reference [14] and in conjunction with the special characteristics of transonic flow, applies the commonly used potential flow approximation assumption and sets up a family of variational principles for three-dimensional transonic steady relative flow with imbedded shocks in an impeller. After combining this with the discontinuous finite element [5], we seek a theoretical basis for developing a new computational method which allows the various unknown flow discontinuities (including shock and free trailing vortex sheets) to be singled out automatically and distinctly.

II. The Aerodynamic System of Equations and Boundary Conditions of a Steady Relative Flow in a Rotating Impeller

Here we will consider the ideal gas for making a steady three-dimensional adiabatic flow in a system with a fixed angle of velocity W rotating around a Z axis (see fig.1).

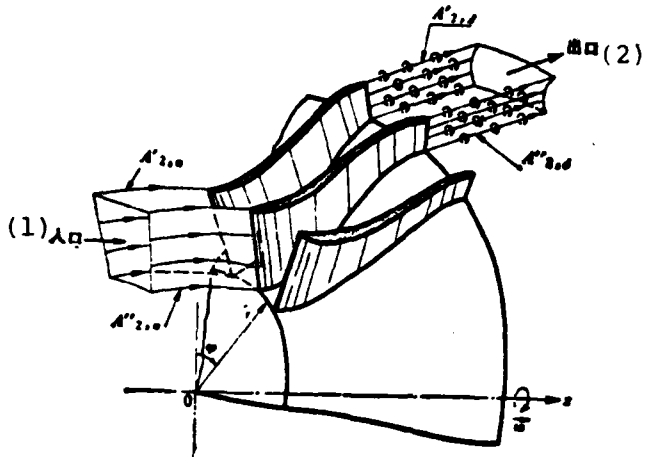

Fig. 1 Three Dimensional Relative Flow Field in a Rotating Impeller

Key: 1. Entrance
2. Exit

Due to the fact that the entropy gradient after the curve shock can usually be considered very small in the transonic area, we can approximate that the flow field has equal entropy (i.e. $\nabla s=0$). If the gas entering in front of the rotating impeller has absolutely no rotation ($\nabla \times c_1=0$) and generalized enthalpy (or stagnation rotor enthalpy) $R=i+\frac{w_2}{2}-\frac{w^2 r^2}{2}$ is homogeneous (i.e. $\nabla R_1=0$), then from the gas flow equation [1], $w \times (\nabla \times c) = \nabla R - T \nabla s$, and the Thomson theorem we know that the flow in this rotating impeller will maintain absolute non-rotation everywhere, that is, $\nabla \times c \equiv 0$. We know from this that there must exist a velocity potential function $\Phi(r, \varphi, z)$.

1. The Aerodynamic System of Equations

The aerodynamic system of equations for the above mentioned flow can be written, in the cylindrical coordinate system (r, φ, z) fixed on a rotor, into dimensionless forms as follows [1]:

$$r \cdot \nabla \cdot (\tilde{\rho}\Lambda) = \frac{\partial(\tilde{\rho} r \Lambda_r)}{\partial r} + \frac{\partial(\tilde{\rho}\Lambda_\varphi)}{\partial \varphi} + \frac{\partial(\tilde{\rho} r \Lambda_z)}{\partial z} = 0 \tag{1}$$

$$\left.\begin{aligned} &\frac{\partial \Phi}{\partial r} = \frac{c_r}{a_0} = \frac{w_r}{a_0} = \Lambda_r \qquad \frac{\partial \Phi}{\partial \varphi} = \frac{c_u}{a_0} r = (\Lambda_\varphi + \Lambda_u) r \\ &\frac{\partial \Phi}{\partial z} = \frac{c_z}{a_0} = \frac{w_z}{a_0} = \Lambda_z \end{aligned}\right\} \tag{2}$$

$$\tilde{\rho} = \tilde{p}^{\frac{1}{k}} = \tilde{a}^{\frac{2}{k-1}} = \left\{1 - \frac{1}{2m}(\Lambda^2 - \Lambda_z^2)\right\}^m \tag{3}$$

Here, besides the generalized enthalpy modified use of the symbol R, we used dimensionless quantities and symbols similar to those of reference [8]. We could also use equation (2) to eliminate the Λ in equations (1) and (3) and obtain two equations which only contain Φ and p (or $\tilde{a}$) as shown below [1]:

$$\begin{aligned} &(1 - M_r^2)\frac{\partial^2 \Phi}{\partial r^2} + \frac{1 - M_\varphi^2}{r^2}\frac{\partial^2 \Phi}{\partial \varphi^2} + (1 - M_z^2)\frac{\partial^2 \Phi}{\partial z^2} - \frac{2M_r M_\varphi}{r}\frac{\partial^2 \Phi}{\partial r \partial \varphi} \\ &- \frac{2M_\varphi M_z}{r}\frac{\partial^2 \Phi}{\partial \varphi \partial z} - 2M_z M_r \frac{\partial^2 \Phi}{\partial z \partial r} + \frac{1 + (M_\varphi + M_u)^2}{r}\frac{\partial \Phi}{\partial r} = 0 \end{aligned} \tag{1'}$$

$$\tilde{a}^2 = \tilde{p}^{\frac{1}{m}} = \left\{1 - \frac{1}{2m}\left[\left(\frac{\partial \Phi}{\partial r}\right)^2 + \left(\frac{1}{r}\frac{\partial \Phi}{\partial \varphi} - \Lambda_u\right)^2 + \left(\frac{\partial \Phi}{\partial z}\right)^2 - \Lambda_z^2\right]\right\} \tag{3'}$$

In the equations

$$\left.\begin{aligned}
M_r &= \frac{w_r}{a} = \frac{\Lambda_r}{\tilde{a}} = \frac{1}{\tilde{a}}\frac{\partial \Phi}{\partial r} = \frac{1}{\beta^{\frac{1}{2m}}}\left(\frac{\partial \Phi}{\partial r}\right) \\
M_\varphi &= \frac{w_\varphi}{a} = \frac{\Lambda_\varphi}{\tilde{a}} = \frac{1}{\tilde{a}}\left(\frac{1}{r}\frac{\partial \Phi}{\partial \varphi} - \Lambda_u\right) = \frac{1}{\beta^{\frac{1}{2m}}}\left(\frac{1}{r}\frac{\partial \Phi}{\partial \varphi} - \Lambda_u\right) \\
M_z &= \frac{w_z}{a} = \frac{\Lambda_z}{\tilde{a}} = \frac{1}{\tilde{a}}\frac{\partial \Phi}{\partial z} = \frac{1}{\beta^{\frac{1}{2m}}}\frac{\partial \Phi}{\partial z} \\
M_u &= \frac{u}{a} = \frac{\Lambda_u}{\tilde{a}} = \frac{\Lambda_u}{\beta^{\frac{1}{2m}}}
\end{aligned}\right\} \qquad (3'')$$

Aside from this, we could also substitute equations (3') and (3") into equation (1') and obtain an equation which only contains Φ .

2. Conditions on the Boundaries and on the Discontinuities

We will only discuss the boundary conditions for whole impellers which have not yet reached a state of complex blockage.

Letting A_1 represent the section (area) of the impeller's entrance and exit as well as the entire solid wall surface (above it there is possibly gas suction or blowing) of a flow path in an impeller (fig. 1); using $A'_{2,u}$ and $A''_{2,u}$ to indicate a cascade's upstream cycle reference boundary surface, the cycle distance between the two is an angular segment distance $\Delta\varphi = 2\pi/N$ and here N is the blade number; using $A'_{2,d}$ and $A''_{2,d}$ to indicate the cascade's downstream cycle boundary surface (free trailing vortex sheet), the cyclic distance between the two is $\Delta\varphi$. Using A_s to indicate the shock, Σ to indicate the artificial interface, and A to indicate the whole boundary surface: $A=A_1 \cup A_2 \cup A_s \cup \Sigma$. The subscript

pr is used to indicate the given quantity. Therefore, the boundary conditions can be expressed as follows:

1) On the A_1 surface. The given normal direction dense flow distribution.

$$\tilde{\rho}\Lambda_n = (q_n)_{pr} \tag{4}$$

It shows that there is a fixed distribution of blowing (suction) gas on the outside (wall) surface.

2) On the A_2 surface. On the upstream $A_{2,u}$, there is cyclicity of all of the air flow parameter along the perimeter and the angular segment distance $\Delta\varphi$ is the cycle. The velocity potential Φ is then indicated with the following equation:

$$\Phi(r, \varphi \pm k \cdot \Delta\varphi, z) = \Phi(r, \varphi, z) \pm k \cdot \Delta\Phi_n \quad (k = 0, 1, 2, \cdots) \tag{5}$$

In this equation, $\Delta\Phi_u = \Phi''_{2,u} - \Phi'_{2,u}$ is the given value. On the downstream $A_{2,d}$ (free trailing vortex sheet) in the parameters of the two sides (indicated separately by "+" and "-") there is the following two joined conditions [6,7]:

$$\left.\begin{aligned} p_- &= p_+ \quad (\text{即 } \Lambda_- = \Lambda_+) \\ (\Lambda_n)_- &= (\Lambda_n)_+ = 0 \end{aligned}\right\} \tag{6}$$

Noting that Λ_+ and Λ_- are different directions, if we let $\Sigma\Lambda = \Lambda_- + \Lambda_+$, and $\Delta\Lambda = \Lambda_+ - \Lambda_-$, then when the trailing vortex strength is equal to $|\Delta\Lambda|$ and the

direction is perpendicular with $\Delta\Lambda$ then it is parallel with $\Sigma\Lambda$. Because of this, generally speaking, the components of Λ_- and Λ_+ always show outstanding discontinuities on the free trailing vortex surface. Theoretically, the blade's downstream must always be able to show a free trailing vortex surface for all of the non-free vortex flow type impellers. At this time, it is only necessary to accord with the general Kutta-Жуковский conditions (abbreviated as the K-J conditions) [14] and equation (6) in order to derive the position and flow field of the free trailing vortex surface. After this, we can then determine $\Delta\Phi_d (= \Phi''_{2,d} - \Phi'_{2,d})$. Actually, in order to satisfy the K-J conditions, we can make the starting line of the free trailing vortex surface on a high designated trailing edge stationary point position along the blade.

3) On the A_s surface. It should satisfy the shock discontinuity conditions [15].

$$\left.\begin{aligned} &(\rho w_n)_- = (\rho w_n)_+ \\ &p_- - p_+ = (\rho w_n^2)_+ - (\rho w_n^2)_- \\ &(w_\tau)_- = (w_\tau)_+ \\ &R_- = R_+ \end{aligned}\right\} \qquad (7A)$$

From this, we can deduce the well-known Rankine-Hugoniot conditions.

$$\frac{p_+}{p_-} = \frac{\frac{k+1}{k-1}\left(\frac{\rho_+}{\rho_-}\right) - 1}{\frac{k+1}{k-1} - \left(\frac{\rho_+}{\rho_-}\right)} \qquad (7B)$$

Here, the subscripts "-" and "+" separately indicate the aerodynamic parameters of the shock's front and back sides.

III. The Variational Principles for Three-Dimensional Transonic Flow

We can set up the following variational principles for the above mentioned three-dimensional flow. The solution of a three-dimensional transonic flow with embedded shocks in a rotating impeller is equivalent to the extreme value necessary conditions of the following function $J(\Phi)$:

$$\delta J = 0$$

$$J(\Phi) = \iiint_{(V)} F\left(\frac{\partial\Phi}{\partial r}, \frac{\partial\Phi}{\partial\varphi}, \frac{\partial\Phi}{\partial z}, r\right) r \cdot dr \cdot d\varphi \cdot dz + \iint_{(A_1)} (q_\infty)_{rr}, \Phi \cdot dA - \iint_{(A'_{2,u})} (\Phi'' - \Phi' - \Delta\Phi)(\rho A_n)' \cdot dA - \iint_{(\Sigma)} (\Phi_+ - \Phi_-)(\rho A_n)_+ \cdot dA \qquad (8)$$

In the equation

$$F = \frac{\tilde{p}}{k} = \frac{1}{k}\left\{1 - \frac{1}{2m}\left[\left(\frac{\partial\Phi}{\partial r}\right)^2 + \left(\frac{1}{r}\frac{\partial\Phi}{\partial\varphi}\right)^2 + \left(\frac{\partial\Phi}{\partial z}\right)^2 - 2\frac{A_u}{r}\frac{\partial\Phi}{\partial\varphi}\right]\right\}^{k=}$$

See fig. 1 for the $A'_{2,u}$ and $A''_{2,u}$ surfaces. The symbols "$'$" and "$''$" separately indicate the parameters of the A'_2 and A''_2 surfaces, (V) indicates the solution domain, and ∂ indicates the position vector of the interface element dA.

[Proof] When we take the variations of equation (8) and allow each position of the unknown discontinuities to be free variations, we should therefore use the variations with variable domain equation (I-4) in the Appendix and should use stronger conditions $\Phi_+ = \Phi_-$ for shock surface A_s. Because variables $\delta\Phi$ and $\delta\mathcal{S}$ are completely arbitrary, from δ J=0 we can thus obtain the following complete set of

extreme value necessary conditions:

The Euler equation: $\nabla \cdot (\tilde{\rho} \Lambda) = 0$ (which continues equation (1) or (1')).

Group of natural boundary conditions:

1) On A_1 surface

$$\tilde{\rho} \Lambda_n = (q_n)_{pr}$$

2) On the $A'_{2,u}$ and $A''_{2,u}$ surfaces

$$(\tilde{\rho} \Lambda_n)' = (\tilde{\rho} \Lambda_n)'', \quad \Phi'' = \Phi' + \Delta \Phi_n$$

From this it can be inferred that their tangential flow rates must be equal, and furthermore from equation (3) we know that $\tilde{\rho}, \Lambda$ and all aerodynamic are all equal.

3) On the $A_{2,d}$ surface

$$(\tilde{\rho} \Lambda_n)' = (\tilde{\rho} \Lambda_n)'' = 0, \quad \tilde{p}' = \tilde{p}''$$

4) On the Σ surface

$$(\tilde{\rho} \Lambda_n)_- = (\tilde{\rho} \Lambda_n)_+, \quad \Phi_- = \Phi_+$$

From this we can deduce that all of the aerodynamic parameters are continuous.

5) On the A_s shock surface

$$\left.\begin{aligned} &(\tilde{\rho} \Lambda_n)_- = (\tilde{\rho} \Lambda_n)_+ \\ &\left(\frac{\tilde{p}}{k} + \tilde{\rho} \Lambda_n^2\right)_- = \left(\frac{\tilde{p}}{k} + \tilde{\rho} \Lambda_n^2\right)_+ \end{aligned}\right\} \qquad (9a)$$

On the A_s surface, besides these two natural boundary conditions, there are also two related equations. The first is the above used strong condition $\Phi_- = \Phi_+$ and thus $\left(\frac{\partial \Phi}{\partial \tau}\right)_- = \left(\frac{\partial \Phi}{\partial \tau}\right)_+$ wherein the tangent flow velocity is equal to

$$(\Lambda_\tau)_- = (\Lambda_\tau)_+ \qquad (9b)$$

The other related equation is the generalized enthalpy non-changing conditions

$$R_- = R_+ \qquad (9c)$$

This is also the non-changing relatively stagnant enthalpy $(i_w^*)_- = (i_w^*)_+$.

Because the entropy increases in transonic flow form a direct ratio with shock strength of the third degree, it is only necessary for the Mach number before the shock to not be much higher than one. Then the entropy increase after a shock will be very small and the changes of p_o and ρ_o can be disregarded. Therefore, the natural boundary conditions of equation (9a) can, along with the conditions of equations (9b) and (9c), represent the shock discontinuities conditions of equation (7A) and the Rankine-Hugoniot conditions of equation (7B).

Up until now, we have derived from the variational principle $\delta J(\Phi) = 0$ the potential function equation (1') for transonic three-dimensional flow with shock waves in the impeller as well as all of the bojndary conditions (including the discontinuous conditions of the unknown discontinuities). Moreover, all the discontinuities were obtained automatically using the forms of the natural boundary conditions.

IV. Generalized Variational Principle for Three-Dimensional Transonic Flow and Its Derivative Group

1. We can also establish the following generalized variational principle: the solution for the three-dimensional transonic flow with embedded shocks in a rotating impeller is equal to the extreme value necessary conditions (here let Φ, Λ_r, Λ_φ, Λ_z, $\tilde{p}$ and $\tilde{\rho}$ be independent variables of the following functional $J_0(\Phi, \Lambda_r, \Lambda_\varphi, \Lambda_z, \tilde{p}$ and $\tilde{\rho})$

$$J_0(\Phi, \Lambda_r, \Lambda_\varphi, \Lambda_z, \tilde{p}, \tilde{\rho}) = \iiint_{(V)} \hat{F} \cdot r \cdot dr \cdot d\varphi \cdot dz + \iint_{(A_1)} (q_n)_{pr} \Phi \cdot dA$$
$$- \iint_{(A'_{2+n})} (\Phi'' - \Phi - \Delta\Phi_n)(\tilde{\rho}\Lambda_n)' dA$$
$$- \iint_{(\Sigma)} (\Phi_+ - \Phi_-)(\tilde{\rho}\Lambda_n)_- dA \qquad (10)$$

In the equation

$$-\hat{F} = \tilde{\rho}\left\{\Lambda_r \frac{\partial\Phi}{\partial r} + \frac{\Lambda_\varphi}{r}\frac{\partial\Phi}{\partial\varphi} + \Lambda_z \frac{\partial\Phi}{\partial z} - \frac{1}{2}(\Lambda^2 + \Lambda_u^2 + 2\Lambda_u\Lambda_\varphi)\right\} + \Pi$$
$$\Pi = m\left\{\frac{\tilde{p}}{k}\left[1 - \ln\left(\frac{\tilde{p}}{\tilde{\rho}^k}\right)\right] - \tilde{\rho}\right\}$$

[Proof] Taking the variations ofequation (10), and using the variations with variable domain of formula (I-5) in the Appendix and the strong conditions of $\Phi_- = \Phi_+$, we can derive a complete set of extreme value necessary conditions from $\delta J_o = 0$ as follows:

The Euler equation group. Besides including the four equations in (1) and (2), it also has

$$\frac{\tilde{p}}{\tilde{\rho}} + \frac{1}{2m}\left(\Lambda^2 - \Lambda_u^2\right) = 1 \quad \text{(energy equation)}$$

$\tilde{p} = \tilde{\rho}k$ (uniform entropy relation)

They are equivalent to formula (3).

The natural boundary condition group. This is completely identical to the previous variational principle.

2. Subgeneralized variational principle group

Following the conversion method found in reference [8], we can derive a family of subgeneralized variational principles from this generalized variational principle. We will not repeat the individual examples here but only point out that among them there is also included the above mentioned variational principle of $\delta J(\Phi)=0$.

V. Conclusion

In the above section we established a family of variational principles for transonic steady relative flow with embedded shocks in a rotating impeller. Its special feature was taking full advantage of natural boundary conditions and all of the boundary conditions (including the discontinuous conditions on the various unknown discontinuities) were converted into natural ones. This provided a theoretical basis for a new computational method and after being combined with the discontinuous finite element [5] as well as the special handling of the supersonic domain we were able to use the finite element method to automatically and distinctly compute the various unknown discontinuities in the flow field.

Naturally, the results of this article are likewise applicable for static three-dimensional cascades as well as various internal flows (for example, various curved flow channels such as nozzles, diffusers, impeller intake and exhaust pipes) and various external flow [7] problems.

The results of this paper can be viewed as extensions of the variational principles found in reference [8] and as related in

sections II and IV to three-dimensional conditions.

References

[1] Wu Chung-Hua, NACA, TN2604 (1952).

[2] Laskaris, T.E., AIAA-Journal, 16, 7(1978).

[3] Denton, J., ARC, R & M 3775 (1974).

[4] Xin Xiaokang and Jiang Jinliang, Mechanics, 2(1977)

[5] Oden, J.T. et al, Computational Mechanics, Lecture Notes in Mathematics, 461. Springer-Verlag (1975).

[6] Mangler, K.W., In: Hewitt et al., Computational Methods and Problems in Aeronautical Fluid Dynamics (1976).

[7] Weber, J.A. et al., AIAA-Journal, 14, 4(1976).

[8] Liu Gaolian, Acta Mechanica Sinica, 4(1979).

[9] Chan, S.K.T. et al., AIAA Paper, 75-79 (1975).

[10] Wang, C.T. & Chow, P.C., NACA, TN 2539 (1951).

[11] Carey, G.F., Computer Methods in Appl. Mech. & Engrg. 13, 2(1978).

[12] Serrin, J., Mathematical Principles of Classical Fluid Mechanics, In: Flügge, S., et al, Handbuch der Physik. Bd. VIII/1, Strömungsmechanik I, (1959).

[13] Courant, R. & Hibert, D., Methodes of Math. Physics I(1953).

[14] Liu Gaolian, Variational Principles for Three-Dimensional Relative Flows of Gas in an Impeller, Research Report of the Shanghai Institute of Mechanical Engineering, (1980).

[15] Xu Jianzhong, The Shock Relation in an Impeller, Work Report of the Mechanics Institute, Chinese Academy of of Sciences (1978).

Appendix Analogy Between the Functional Variations With Variable Domain and the Reynold's Transport Theorem

Below we will point out the analogy and relationship between variations with variable domain and the Reynold's transport theorem. Furthermore, we will use it to provide a simple and convenient method for solving the problem of variations with

variable domain. Because the Reynold's transport theorem represents the relationship of the control and closed systems, we can use a mechanical method to derive it. Therefore, this method is more directly perceivable than most methods [13] which use mapping (conversion) and it also gives variations with variable domain a certain physical (analogous) significance.

First, Reynold's transport theorem expresses moving liquids which use a flow velocity w' [12] as:

$$\frac{D}{Ds}\iiint_{(V)} F \cdot dV = \iiint_{(CV)} \frac{\partial F}{\partial s} \cdot dV + \oint_{(CS)} F \cdot (w' \cdot dA) \qquad (1\text{-}1)$$

In this equation, (CS) indicates the control surface, dV is the infinitesimal volume, dA is the infinitesimal surface area, the normal direction n outside the (CS) is taken as regular, and $F=F(r, \varphi, z, s)$ is an arbitrary function.

We can compare the variations of the area to the position changes of the closed system (V). The position changes depend on the time parameter t. Therefore, for the arbitrary variable Q, we can separately write the following formulas for its variations with fixed domain $\tilde{\delta} Q$ and variations with variable domain δQ :

$$\tilde{\delta} Q = \left(\frac{\partial Q}{\partial s} \cdot s\right)_{t=\text{const}}, \quad \delta Q = \left(\frac{DQ}{Ds} \cdot s\right)_{t=\text{const}}$$

Naturally, the (CS) moving velocity w' can be indicated by its displacement DS'

$$(w', i)_{t=0} = \left(\frac{D\delta\vec{r}}{Dt} \cdot i\right)_{t=0} = \delta\vec{r} = i_r \cdot \delta r + i_\varphi r\delta\varphi + i_z \cdot \delta z$$

and

$$dA = n \cdot dA = \left(i_r \frac{\partial r}{\partial n} + i_\varphi r \frac{\partial \varphi}{\partial n} + i_z \frac{\partial z}{\partial n}\right) dA$$

After using t to multiply each item in equation (I-1), taking the limit as $t \to 0$, and taking into account the above equations, we obtain

$$\delta \iiint_{(V)} F \cdot dV = \iiint_{(CV)} \delta F \cdot dV + \oint_{(CS)} F(\delta\vec{r} \cdot n) dA$$
$$= \iiint_{(CV)} \delta F \cdot dV + \oint_{(CS)} F\left(\frac{\partial r}{\partial n}\delta r + \frac{\partial \varphi}{\partial n} r^2 \delta\varphi + \frac{\partial z}{\partial n}\delta z\right) dA$$

Letting $J = \iiint_{(V)} F dV$, then its fixed domain and variable domain variations can be separately expressed as

$$\bar{\delta} J = \iiint_{(CV)} \delta F \cdot dV, \quad \delta J = \delta \iiint_{(V)} F \cdot dV$$

After substituting in the above equation, we can obtain

$$\delta J = \bar{\delta} J + \oint_{(CS)} F(\delta\vec{r} \cdot n) dA \qquad (I-2)$$

In this equation

$$\delta J = \iiint_{(CV)} \left\{ \frac{\partial F}{\partial \Phi} \delta\Phi + \frac{\partial F}{\partial \Phi_r} \delta\Phi_r + \frac{\partial F}{\partial \left(\frac{\Phi_\varphi}{r}\right)} \cdot \delta\left(\frac{\Phi_\varphi}{r}\right) + \frac{\partial F}{\partial \Phi_z} \delta\Phi_z \right\} dV$$

and

$$\Phi_r = \frac{\partial \Phi}{\partial r}, \quad \Phi_\varphi = \frac{\partial \Phi}{\partial \varphi}, \quad \Phi_z = \frac{\partial \Phi}{\partial z}$$

Introducing vector G

$$G = \frac{\partial F}{\partial \Phi_r} i_r + \frac{\partial F}{\partial \left(\frac{\Phi_\varphi}{r}\right)} i_\varphi + \frac{\partial F}{\partial \Phi_z} i_z$$

Moreover, after applying the Gauss theorem, we can write $\tilde{\delta} J$ as

$$\tilde{\delta} J = \iiint_{(CV)} \left\{ \frac{\partial F}{\partial \Phi} - \operatorname{div} G \right\} \delta\Phi \cdot dV + \oint_{(CS)} (G \cdot n) \tilde{\delta}\Phi \cdot dA$$

After substituting in equation (I-2), we obtain

$$\delta J = \iiint_{(CV)} \left(\frac{\partial F}{\partial \Phi} - \nabla \cdot G \right) \delta\Phi \cdot dV + \oint_{(CS)} (G \cdot \tilde{\delta}\Phi + P \cdot \delta\Phi') \cdot n dA \qquad (I-3)$$

Here, $\tilde{\delta}\Phi$ is the fixed Φ variation on (CS). In order to make it practical and convenient, the $\delta\Phi$ variation along the variable domain peripheral interface should be used to replace it.

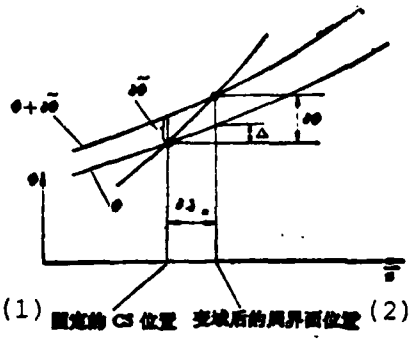

Fig. 2 The Variations of Function Φ Along the Outside Normal Direction

Key: 1. Fixed CS position
2. Peripheral interface position after the variable domain

From fig. 2 we know that $\delta\Phi = \tilde{\delta}\Phi + \Delta = \tilde{\delta}\Phi + \frac{\partial\Phi}{\partial n}\delta\mathcal{S}$, and after substituting in formula (I-3), we obtain a general formula for variations with variable domain

$$\delta J = \iiint_{(CV)} \left(\frac{\partial F}{\partial \Phi} - \nabla \cdot G\right)\delta\Phi \cdot dV + \oint_{(CS)} \left\{G_n \cdot \delta\Phi + \left(F - G_n \frac{\partial\Phi}{\partial n}\right)\delta\mathcal{S}_n\right\} dA \qquad (I-4)$$

When F contains many unknown function Φ^j (j=1,2,3...), then

$$\delta J = \iiint_{(CV)} \sum_j \left[\left(\frac{\partial F}{\partial \Phi^j} - \nabla \cdot G^j\right)\delta\Phi^j\right] dV + \oint_{(CS)} \sum_j \left\{G_n^j \cdot \delta\Phi^j + \left(F - G_n^j \frac{\partial\Phi}{\partial n}\right)\delta\mathcal{S}_n\right\} dA \qquad (I-5)$$

VARIATIONAL PRINCIPLES AND GENERALIZED VARIATIONAL PRINCIPLE FOR THREE-DIMENSIONAL TRANSONIC FLOW WITH SHOCK WAVES IN A ROTATING TURBO-IMPELLER

Liu Gaolian

(Shanghai Institute of Mech. Engineering)

Abstract

In this article a family of variational principles for 3D transonic steady relative flow with embedded shocks in a turbomachine impeller of axial, radial or mixed flow type is developed. Its special feature is to take full advantage of natural boundary conditions and "artificial interfaces," so as to facilitate the handling of various complex boundary conditions. As a result, all boundary conditions in the problem under study have been converted into natural ones Moreover, it is also shown that by taking variations of the position of unknown flow discontinuities (such as shocks, free trailing vortex sheets all matching conditions across these discontinuities, including the well-known Rankine-Hugoniot shock relation, can be derived from the variational principles as natural interface-conditions.

This article is primarily intended to provide, in conjunction with the discontinuous finite element[3], a theoretical basis for developing a novel computational method, which allows all flow discontinuities to be singled out automatically and distinctly (without smearing). Owing to the assumption of the existence of a velocity potential, the applicability of the present theory is limited to cases where Mach numbers before the shock do not differ greatly from one. The variational principles presented herein are some extension of those developed previously in [8].

In the appendix, an analogy between the functional variations with variable domain and the Reynolds' transport theorem is pointed out and used as a basis for deriving a general formula for such variations.

CALCULATION FOR THREE-DIMENSIONAL TURBULENT BOUNDARY LAYER ON A YAWED WING IN COMPRESSIBLE FLOW

by Zhang Guofu
(Nanjing Institute of Aeronautics)

Abstract

This paper starts from the equations of motion in generalized curvilinear coordinates and the model of Head's two-dimensional entrainment theory, and derives a set of equations along surface curve on normal profile of a yawed wing for a compressible three-dimensional turbulent boundary layer. After a typical form of a set of ordinary differential equations with initial values is obtained by matrix transformation we solved these equations by numerical computation.

Thompson and MacDonald's computational results on flow around an attachment line in the leading edge of a yawed wing have been used as the initial values to solve the set of ordinary differential equations.

The method in this paper can be used to calculate the separation position of boundary layer, various boundary layer thicknesses and wall stress, and describe the difference between streamlines outside the boundary layer and streamlines on the wall.

Typical computations show that the present method agrees well with experimental results.

Primary Symbols

U_c local composite velocity on boundary layer

u, v, w velocity in ξ, n, ζ directions

u_1, v_1 component velocity of U_c in x,y directions

β lateral stream angle (fig. 1)

ε local stream line angle (fig. 2)

K $= tg\varepsilon$

$\tau_1 \tau_2$ shearing stress along ξ and η directions

τ_w wall shearing stress

τ_{w1}, τ_{w2} τ_w components in the ξ and η directions

c_f $\tau_w / (\frac{1}{2} \rho_e U_e^2)$, friction coeffient

c_{f1} $= c_f \cos\beta$, the friction coefficient in the main stream direction outside the boundary layer

c_{f2} $= c_f \cos\beta$, the friction coefficient in the lateral stream direction

v air motion viscosity coefficient

Λ wing's angle of yaw

c normal wing profile chord length

δ thickness of boundary layer

δ_1 $= \int_o^s (1 - \frac{\overline{\rho u}}{\rho_e U_e})$ displacement thicknesses in $d\xi$ and η directions

δ_2 $= - \int_o^\delta \frac{\overline{\rho v}}{\rho_e U_e}$ displacement thicknesses in d

and directions

θ_{11} $= \int_o^\delta (1 - \frac{\overline{u}}{U_e}) \frac{\overline{\rho u}}{\rho_e U_e}$ momentum loss thicknesses in $d\zeta$ and ξ directions

θ_{22} $= - \int_o^\delta \frac{\overline{\rho v v}}{p_e U_e^2}$ momentum loss thicknesses in $d\zeta$ and η directions

$$\theta_{12} = \int_0^{\delta} \frac{\overline{\rho v}}{\rho_e U_e} \left(1 - \frac{\bar{u}}{U_e}\right) d\zeta$$

$$\theta_{21} = -\int_0^{\delta} \frac{\overline{\rho uv}}{\rho_e U_e^2} d\zeta$$

} mixed momentum loss thicknesses

$$R_{\theta_{11}} = (U_e \theta_{11})/V_e$$

$$Z_1 = \theta_{11} \cdot (d\beta/dx)$$

$$C^* = \frac{V_{e,1}^2 \sin^2 \Lambda}{V_{e,1} \cdot \left(\frac{du_1}{dx}\right)_{a,1}}$$

attachment line in air stream with similar parameters

$$H = \delta_1 / \theta_{11}$$

$$\bar{H} = \frac{1}{\theta_{11}} \int_0^{\delta} \frac{\rho}{\rho_e} \left(1 - \frac{u}{u_e}\right) d\zeta$$

compressibility analogy of $d\zeta$ and H

$$H_1 = (\delta - \delta_1)/\theta_{11}$$

Footnotes

a.l	attachment line value
e	potential flow value of boundary layer
w	wall value

A lateral line on top of a symbol indicates a time average value and one with a left-falling stroke indicates a pulsating value.

I. Foreward

In recent years, due to developments in aviation, especially those in transonic flight technology, aerodynamics is daily confronted with the serious challenge of separated flow. For example, in mechanism, the solution of the problem of transonic buffeting being totally different from low speed buffeting always possesses a decisive

effect on the economic performance of the transporter (buffeting boundary) or on the mobility performance of a fighter (buffeting performance).

When the boundary layer theory is used to handle the problem of three-dimensional wing separation, even the simplest calculation of an unlimited yawed wing boundary layer is much more difficult than for a profile. There are two main reasons for this: (1) When considering the viscosity of the flow around an unrestrained yawed wing, the calculation results for a normal profile can usually be directly converted to a yawed wing in accordance with the law of cosines. Yet, when handling the related viscosity problems, in principle the law of cosines is not established. This is because the S shaped curved stream line outside the boundary layer not only causes the inside of the boundary layer to have the same velocity as the main stream direction outside the boundary layer but the inside also has the same vertical velocity as the main stream (fig. 1).

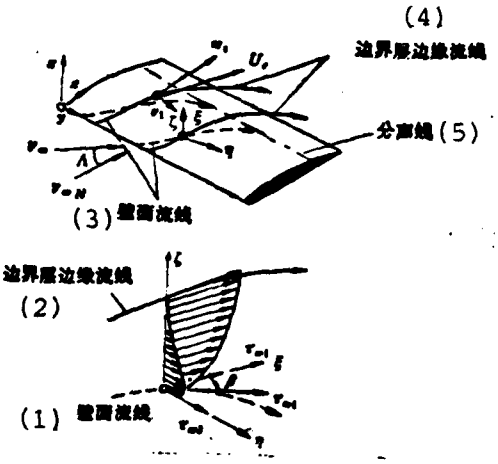

Fig. 1

Key: 1. Wall stream line
2. Boundary layer stream line
3. Wall stream line
4. Boundary layer stream line
5. Separating line

Therefore, the stream within the boundary layer is three-dimensional. Concurrently, the wall stream line is not identical to the boundary layer stream line and the included angle between them is β. Any one point on the wall takes the coordinates ξ, η, ζ; ξ is the stream line direction along the boundary layer, η is vertical to ξ along the wall and ζ is upward vertical to the wall. Fig. 1 draws the main stream direction velocity $u(\zeta)$ and the lateral stream direction velocity $v(\zeta)$ with the corresponding wall friction stresses of τ_{w1} and τ_{w2}. The total friction stress is thus $\tau_w = \tau_{w1} + \tau_{w2}$. The wall stream line direction is defined as identical to the τ_w direction. Generally, Redeker [1] points out, for a wing with a relatively large angle of sweepback ($\Lambda > 30^\circ$), there is separation when the wall stream line is parallel to the trailing edge. Although, at this time, the wall stress is not equal to zero, yet for a relatively small wing, the occurence of separation is often already $\tau_w = 0$ before the wall stream line is parallel to the trailing edge. This is analogous to a two-dimensional situation. (2) When the air stream flows along the leading edge of the yawed wing, two branches are formed on the attachment line, one branch goes up while the other goes down. This phenomenon is analogous to the air stream flowing gradually passed and closer to a drawing in flat boundary layer. Based on the test results of Cumpsty and Head [2], when $R_{\theta_{11}} > 100$ is on the attachment line, there is a turbulent boundary layer. When modern large scale transporters are cruising, they generally exceed this value and therefore we can consider that there is a turbulent boundary layer on the attachment line. By utilizing a series of dominant equations for the turbulent boundary layer and integrating the special characteristics of the stream on the attachment line, we can calculate the air stream parameters on

the attachment line. Crumpty and Head [2] initially calculated uncompressible results but compressible and more practical results were subsequently presented by Thompson [3].

Due to the difficulties of test research and analysis of the above mentioned theory, progress in this area has been slow. Not until the 1970's did we begin seeing research papers on large swept back wings with compressible turbulent boundary layers. Yet, some papers only present formula results and others are merely limited to discussing specialized problems. They lack systematic formula demonstration and calculation methods. In addition, many errors have been found in the formulas published. In view of the above mentioned facts, this article starts from the equations of motion in generalized curvilinear coordinates and the model of Head's two-dimensional entrainment theory and derives a set of dominant equations for the stream line in the curvilinear coordinates along the boundary layer. The results are basically the same as those found in reference [1]. Redeker [1] used repeated iteration to solve the above mentioned set of equations. Afterwards, Thompson's [3] research showed that the iterative method could have divergent problems when applied to the leading edge of a relatively large wing with an accelerating pressure gradient. Moreover, convergence was very slow near the separation area. We think that, practically speaking, to carry out numerical calculations of the stream line along the outside of the boundary layer is not as convenient as along the normal profile curve and therefore, in this paper, we have carried out variable substitution and matrix operation so as to obtain a typical form of a set of ordinary differential equations with initial values along the normal profile curve. The velocity and wall friction stress formula selected in this article; used the conditions on the attachment line given in reference [3] as initial values; used numerical computations for their solution.

As regards a correctly designed transonic wing, wing root and wing tip modifications should be carried out so as to maintain as best as possible the uniformity of their isobaric lines and equal percentage chord lines. This will cause the greater area on the transonic swept back wing to possess unrestrained yawed wing qualities. Therefore, the boundary layer results from research on the unrestrained yawed wing will have real significance.

II. Set of Dominant Equations For a Turbulent Boundary Layer With Curvilinear Coordinates

We can rewrite the equation of single quality gas motion in generalized curvilinear coordinates presented in reference [4] for situations with applied force (including pressure and tangential force) as

$$\frac{1}{h_i}\left[\frac{d}{dt}\left(\frac{\partial T}{\partial \dot{q}_i}\right)-\frac{\partial T}{\partial q_i}\right]=-\frac{1}{\rho h_i}\frac{\partial p_i}{\partial q_i}+F_i \qquad (1)$$

In the equation, q_i is the generalized curvilinear coordinate, $\dot{q}_i$ is the derivative of q_i for time t, F_i is the tangential force working in the i direction component on the single quality gas, T represents the kinetic energy of the single quality gas, and h_i is the Lamé coefficient along the coordinate q_i. Then

$$T=\frac{1}{2}\sum_{i=1}^{3}h_i^2\dot{q}_i^2=f(q_1, q_2, q_3, \dot{q}_1, \dot{q}_2, \dot{q}_3) \qquad (2)$$

Taking the orthogonal curvilinear coordinates ξ, η and ζ shown in fig. 1 and letting $h_3=1$, from formula (2) we then obtain

$$\frac{\partial T}{\partial q_i} = \frac{u^2}{h_1}\frac{\partial h_1}{\partial q_i} + \frac{v^2}{h_2}\frac{\partial h_2}{\partial q_i} \tag{3}$$

$$\frac{d}{dt}\left(\frac{\partial T}{\partial \dot{q}_i}\right) = \sum_{j=1}^{3}\frac{u_j}{h_j}\left(u_j\frac{\partial h_j}{\partial q_i} + h_j\frac{\partial u_j}{\partial q_i}\right) + h_i\frac{\partial u_i}{\partial t} \tag{4}$$

In formula (1), F_i can be shown by the deformation angle velocity of the curvilinear coordinates [4] and using Prandtl's boundary layer assumption we can obtain

$$F_x = \frac{1}{\rho}\frac{\partial}{\partial \zeta}\left(\mu\frac{\partial u}{\partial \zeta}\right);\quad F_y = \frac{1}{\rho}\frac{\partial}{\partial \zeta}\left(\mu\frac{\partial v}{\partial \zeta}\right) \tag{5}$$

Pressure strength p_i can also be expressed by the pressure strength arithmetic mean p [5] along the three coordinate directions.

In turbulent motion, we can regard the real gas flow parameters as being formed from the superposition of the time average and pulse values, and based on the time averaging principle:

$$\left.\begin{aligned} Z &= \bar{Z} + Z' \\ \overline{ST} &= \overline{(\bar{S}+S')(\bar{T}+T')} = \bar{S}\bar{T} + \overline{S'T'} \end{aligned}\right\} \tag{6}$$

If we substitute formulas (3), (4) and (5) into formula (1), carry out time averaging for formula (6), and then carry out simplification based on Prandtl's boundary layer assumption, we will finally obtain a set of equations of time average motion in curvilinear coordinates for a turbulent boundary layer:

ξ direction momentum equation

$$h_2\overline{\rho u}\frac{\partial \bar{u}}{\partial \xi}+h_1\overline{\rho v}\frac{\partial \bar{u}}{\partial \eta}+h_1h_2\overline{\rho w}\frac{\partial \bar{u}}{\partial \zeta}+\overline{\rho uv}\frac{\partial h_1}{\partial \eta}-\overline{\rho vv}\frac{\partial h_2}{\partial \xi}=-h_2\frac{\partial \bar{p}}{\partial \xi}+h_1h_2\frac{\partial \tau_1}{\partial \zeta} \tag{7}$$

η direction momentum equation

$$h_2\overline{\rho u}\frac{\partial \bar{v}}{\partial \xi}+h_1\overline{\rho v}\frac{\partial \bar{v}}{\partial \eta}+h_1h_2\overline{\rho w}\frac{\partial \bar{v}}{\partial \zeta}+\overline{\rho uv}\frac{\partial h_2}{\partial \xi}-\overline{\rho uv}\frac{\partial h_1}{\partial \xi}-\overline{\rho uu}\frac{\partial h_2}{\partial \eta}=-h_1\frac{\partial \bar{p}}{\partial \eta}+h_1h_2\frac{\partial \tau_2}{\partial \zeta} \tag{8}$$

In the formulas

$$\tau_1=\mu(\partial\bar{u}/\partial\zeta)-\overline{(\rho w)'u'} \tag{9}$$

$$\tau_2=\mu(\partial\bar{v}/\partial\zeta)-\overline{(\rho w)'v'} \tag{10}$$

The first item on the right side of the above two formulas is the tangential stress caused by viscosity, and the second item is the tangential stress (called Reynold's stress) produced because of the velocity pulse when there is turbulence. Physically, the above results are identical to the conclusion when there are rectangular coordinates.

From the above similar methods we carry out time averaging for the continuous equations [4] of the generalized curvilinear coordinates and obtain

$$\frac{\partial(h_2\overline{\rho u})}{\partial \xi}+\frac{\partial(h_1\overline{\rho v})}{\partial \eta}+h_1h_2\frac{\partial(\overline{\rho w})}{\partial \zeta}=0 \tag{11}$$

If we calculate the ξ coordinate based on the velocity potential, the $d\xi = d\phi$. If along the ξ coordinate $ds=h_1 d\xi$, we obtain

$$h_1 = V_\infty / U_e \tag{12}$$

Then, along the boundary layer, formulas (7) and (8) can be simplified as

$$\left.\begin{aligned} \rho_e \frac{U_e}{h_1}\frac{\partial U_e}{\partial \xi} &= -\frac{1}{h_1}\frac{\partial p}{\partial \xi} \\ \rho_e \frac{U_e}{h_2}\frac{\partial U_e}{\partial \eta} &= -\frac{1}{h_2}\frac{\partial p}{\partial \eta} \end{aligned}\right\} \tag{13}$$

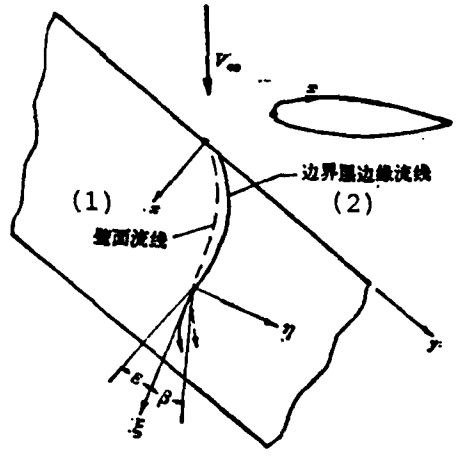

Fig. 2

Key: 1. Wall streamline
2. Boundary layer streamline

As shown in fig. 2, the normal profile curve along the wing takes coordinate x, x begins from the attachment line, and takes coordinate y along the span. The included angle between the wall stream line and boundary stream line is β (lateral

stream angle), and the included angle between the ξ coordinate and x coordinate is ε (local stream line angle). The component velocity of U_e in the x and y directions is u_1 and v_1. Now we will consider the following relations:

(1) Because it is an unrestrained yawed wing and the air stream parameter along the y direction is unchanging, we can obtain

$$\frac{\partial}{h_2 \partial \eta} = -\operatorname{tg}\varepsilon \frac{1}{h_1}\frac{\partial}{\partial \xi} = -K\frac{\partial}{\partial s} = -\frac{v_1}{u_1}\frac{\partial}{\partial s} \qquad (14)$$

(2) Based on the formula defined by θ_{12}, δ_2 and θ_{21}, we obtain

$$\theta_{12} + \delta_2 = \theta_{21} \qquad (15)$$

(3) When we consider compressibility, there is a related formula of the stream line along the boundary layer

$$\frac{1}{\rho_e}\frac{\partial \rho_e}{\partial s} = -M_e^2 \frac{1}{U_e}\frac{\partial U_e}{\partial s} \qquad (16)$$

If we take the thickness integral of each item in formulas (7), (8) and (11) along the boundary layer and substitute them into formulas (12-16), after operation we obtain:

The ξ direction momentum equation

$$\frac{\partial \theta_{11}}{\partial s} + \frac{\theta_{11}}{U_e}\frac{\partial U_e}{\partial s}\left(2 + \frac{\delta_1}{\theta_{11}} - M_e^2\right) - K\frac{\partial \theta_{12}}{\partial s} + \frac{K}{U_e}\frac{\partial U_e}{\partial s} M_e^2 \theta_{12} + \frac{1}{h_1}\frac{\partial h_1}{\partial s}(\theta_{11} - \theta_{22}) = \frac{\tau_{w1}}{\rho_e U_e^2} \qquad (17)$$

The η direction momentum equation

$$\frac{\partial \theta_{21}}{\partial s} + \frac{\theta_{11}}{U_e}\frac{\partial U_e}{\partial s}(2 - M_e^2) + \theta_{21}\frac{2}{h_2}\frac{\partial h_2}{\partial s} - K\frac{\partial \theta_{22}}{\partial s} + \frac{K}{U_e}\frac{\partial U_e}{\partial s} \cdot M_e^2\theta_{22} - \frac{K}{U_e}\frac{\partial U_e}{\partial s}(\theta_{22} + \theta_{11} + \delta_1) = \frac{\tau_{w2}}{\rho_e U_e^2} \tag{18}$$

We took Head's two-dimensional entrainment theory and extended it to a compressible three-dimensional orthogonal curvilinear coordinate system. After the unit area on the boundary surface was put into the gas stream of the boundary layer, we used the entrainment function $F(H_1)$ to express it

$$\frac{1}{U_e}\left(\frac{u_e}{h_1}\frac{\partial \delta}{\partial \xi} + \frac{v_e}{h_2}\frac{\partial \delta}{\partial \eta} - w_e\right) = F(H_1) \tag{19}$$

We took the thickness integrals of each item of the continuous equation (11) along the boundary layer and applied the differentio-integral theorem to obtain

$$\frac{1}{h_1 h_2}\frac{\partial}{\partial \xi}\int_0^\delta \frac{h_2\overline{\rho u}}{U_e}d\zeta + \frac{1}{h_1 h_2}\frac{\partial}{\partial \eta}\int_0^\delta \frac{h_1\overline{\rho v}}{U_e}d\zeta = -\frac{1}{U_e}\left(u_e \cdot \frac{\rho_e}{h_1}\frac{\partial \delta}{\partial \xi} + v_e\frac{\rho_e}{h_2}\frac{\partial \delta}{\partial \eta} - \rho_e w_e\right) \tag{20}$$

If the right side of the above formula is substituted with formula (19), the left side undergoes differential operation and the independent variable position is converted to s, we finally obtain the entrainment equation

$$\frac{\partial(\delta - \delta_1)}{\partial s} + \frac{1}{U_e}\frac{\partial U_e}{\partial s}(1 - M_e^2)(\delta - \delta_1) + \frac{1}{h_2}\frac{\partial h_2}{\partial s}(\delta - \delta_1) + K\frac{\partial \delta_2}{\partial s} - \frac{K}{U_e}\frac{\partial U_e}{\partial s} - M_e^2\delta_2 = F(H_1) \tag{21}$$

In the formula, the entrainment function $F(H_1)$ uses the two dimensional empirical formula

$$F(H_1) = 0.0299(H_1 - 3)^{-0.617} \tag{22}$$

$$H_1 = 1.535(H - 0.7)^{-2.715} + 3.3 \tag{23}$$

In order for the various boundary layer thicknesses in the above formulas to be able to have integration, we had to know the stream velocity and lateral velocity types of the turbulent boundary layers. We used the velocity type formula recommended in reference [3] which calculated the compressibility effect:

The lateral velocity type based on multiplication rate form

$$\frac{u}{U_e} = \left(\frac{Z}{Z_e}\right)^n; \tag{24}$$

The lateral velocity type based on an extension of the non-compressible stream formula

$$\frac{v}{U_e} = \left(1 - \frac{Z}{Z_e}\right)\frac{u}{U_e}\operatorname{tg}\beta \tag{25}$$

In the formula

$$n = (\bar{H} - 1)/2 \tag{26}$$

$$\left.\begin{aligned} \bar{H} &= J_1(H_1)^{(3)} \\ H &= J_2(\bar{H}, M_e)^{(3)} \end{aligned}\right\} \tag{27}$$

From formulas (24) and (25), Green integrated the various boundary layer thicknesses as β, θ_{11} and n functions. After trying formula (26) we obtain

$$\left.\begin{aligned} \theta_{21} &= \operatorname{tg}\beta f_1(\bar{H})\theta_{11}; \quad \theta_{12} = \operatorname{tg}\beta f_2(\bar{H})\theta_{11} \\ \theta_{22} &= \operatorname{tg}\beta f_3(\bar{H})\theta_{11}; \quad \theta_{23} = \operatorname{tg}^2\beta f_4(\bar{H})\theta_{11} \end{aligned}\right\} \tag{28}$$

In the formula

$$\left.\begin{aligned} f_1 &= -2/[(\bar{H}-1)(\bar{H}+2)] \\ f_2 &= (14\bar{H}+30)/[(\bar{H}+2)(\bar{H}+3)(\bar{H}+5)] \\ f_3 &= -16\bar{H}/[(\bar{H}-1)(\bar{H}+3)(\bar{H}+5)] \\ f_4 &= -24/[(\bar{H}-1)(\bar{H}+2)(\bar{H}+3)(\bar{H}+4)] \\ f_2 &= f_1 - f_3 \end{aligned}\right\} \qquad (29)$$

In order for application to be convenient the stream line coordinate s on the outer part of the boundary layer was transformed into the curvilinear coordinate x along the normal profile. We used the divergence formula of the main stream velocity U_e on the boundary layer in the (ξ , η , ζ) and (x,y,z) coordinates.

$$\operatorname{div}(U_e) = \frac{1}{h_1 h_2 h_3}\frac{\partial(U_e h_2 h_3)}{\partial \xi} = \frac{\partial u_1}{\partial x} + \frac{\partial v_1}{\partial y}$$

and obtained

$$\frac{1}{h_1 h_2}\frac{\partial h_2}{\partial \xi} = \frac{1}{U_e}\left(\frac{\partial u_1}{\partial x} + \frac{\partial v_1}{\partial y}\right) - \frac{1}{U_e h_1}\frac{\partial U_e}{\partial \xi} \qquad (30)$$

For the unrestrained yawed wing ($\partial v_1 / \partial y$)=0, and

$$\frac{\partial}{\partial s} = \frac{dx}{ds}\frac{\partial}{\partial x} = \frac{u_1}{U_e}\frac{\partial}{\partial x} \qquad (31)$$

By utilizing the above mentioned relation we then simplified formula (30) into

$$\frac{1}{h_1 h_2}\frac{\partial h_2}{\partial \xi} = \frac{1}{h_2}\frac{\partial h_2}{\partial s} = \frac{v_1^2}{U_e^2}\frac{du_1}{dx} = \frac{1}{U_e^2}\frac{v_1^2}{u_1}\frac{dU_e}{dx} \qquad (32)$$

We substituted formulas (28), (31) and (32) into formulas (17), (18) and (21) and finally obtained a set of dominant equations

$$\begin{pmatrix} K_{11} & K_{12} & K_{13} \\ K_{21} & K_{22} & K_{23} \\ K_{31} & K_{32} & K_{33} \end{pmatrix} \begin{pmatrix} \dfrac{d\theta_{11}}{dx} \\ \dfrac{d\,\mathrm{tg}\,\beta}{dx} \\ \dfrac{d(\delta - \delta_1)}{dx} \end{pmatrix} - \begin{pmatrix} F_1 \\ F_2 \\ F_3 \end{pmatrix} \tag{33}$$

In the formula

$$K_{11} = \frac{u_1}{U_e} - \frac{v_1}{U_e} f_2 \mathrm{tg}\,\beta + \frac{v_1}{U_e} \mathrm{tg}\,\beta \frac{df_2}{d\bar{H}} \frac{d\bar{H}}{dH_1} H_1$$

$$K_{12} = -\frac{v_1}{U_e} f_2 \theta_{11}$$

$$K_{13} = -\frac{v_1}{U_e} \mathrm{tg}\,\beta \frac{df_2}{d\bar{H}} \frac{d\bar{H}}{dH_1}$$

$$K_{21} = \frac{u_1}{U_e} f_1 \mathrm{tg}\,\beta - \frac{v_1}{U_e} f_4 \mathrm{tg}^2\beta - H_1 \frac{d\bar{H}}{dH_1} \left(\frac{u_1}{U_e} \mathrm{tg}\,\beta \frac{df_1}{d\bar{H}} - \frac{v_1}{U_e} \mathrm{tg}^2\beta \frac{df_4}{d\bar{H}} \right)$$

$$K_{22} = \frac{u_1}{U_e} f_1 \theta_{11} - 2 \frac{v_1}{U_e} f_4 \theta_{11} \mathrm{tg}\,\beta$$

$$K_{23} = \frac{u_1}{U_e} \mathrm{tg}\,\beta \frac{df_1}{d\bar{H}} \frac{d\bar{H}}{dH_1} - \frac{v_1}{U_e} \mathrm{tg}^2\beta \frac{df_4}{d\bar{H}} \frac{d\bar{H}}{dH_1}$$

$$K_{31} = \frac{v_1}{U_e} f_3 \mathrm{tg}\,\beta - \frac{v_1}{U_e} \mathrm{tg}\,\beta \frac{df_3}{d\bar{H}} \frac{d\bar{H}}{dH_1} H_1$$

$$K_{32} = \frac{v_1}{U_e} f_3 \theta_{11}$$

$$K_{33} = \frac{u_1}{U_e} + \frac{v_1}{U_e} \mathrm{tg}\,\beta \frac{df_3}{d\bar{H}} \frac{d\bar{H}}{dH_1}$$

$$F_1 = \frac{c_{f1}}{2} - \frac{u_1}{U_e^2} \theta_{11} \left[(H + 2 - \mathrm{M}_e^2) + \frac{v_1^2}{u_1^2} (1 - f_4 \mathrm{tg}^2\beta) + \mathrm{M}_e^2 f_2 \mathrm{tg}\,\beta \frac{v_1}{u_1} \right] \frac{dU_e}{dx}$$

$$F_2 = \mathrm{tg}\,\beta \frac{c_{f1}}{2} + \frac{u_1}{U_e^2} \theta_{11} \left[\mathrm{tg}\,\beta \cdot f_1 \left(\mathrm{M}_e^2 - 2\frac{U_e^2}{u_1^2} \right) + \frac{v_1}{u_1} \left(H + 1 + f_4 \mathrm{tg}^2\beta (1 - \mathrm{M}_e^2) \right) \right] \frac{dU_e}{dx}$$

$$F_3 = F(H_1) + \frac{u_1}{U_e^2} \theta_{11} \left[H_1 \left(\mathrm{M}_e^2 - \frac{U_e^2}{u_1^2} \right) + \mathrm{M}_e^2 \mathrm{tg}^2\beta f_3 \right] \frac{dU_e}{dx}$$

In the formulas, $d\bar{H}/dH_1$, $\bar{H}$ and H can be expressed by formula (27) as the function of H_1. c_{f1} can be expressed by the empirical formula recommended in reference [3].

The set of equations in (33), through matrix transformation, obtained

$$\begin{pmatrix} \frac{d\theta_{11}}{dx} \\ \frac{d\,\mathrm{tg}\,\beta}{dx} \\ \frac{d(\delta-\delta_1)}{dx} \end{pmatrix} = \frac{1}{|K|}\begin{pmatrix} M_{11} & M_{12} & M_{13} \\ M_{21} & M_{22} & M_{23} \\ M_{31} & M_{32} & M_{33} \end{pmatrix}\begin{pmatrix} F_1 \\ F_2 \\ F_3 \end{pmatrix} \tag{34}$$

In the formula

$$\begin{aligned} M_{11} &= K_{22}K_{33} - K_{23}K_{32}, \quad M_{12} = K_{13}K_{32} - K_{12}K_{33} \\ M_{13} &= K_{12}K_{23} - K_{13}K_{22}, \quad M_{21} = K_{23}K_{31} - K_{21}K_{33} \\ M_{22} &= K_{11}K_{33} - K_{13}K_{31}, \quad M_{23} = K_{13}K_{21} - K_{11}K_{23} \\ M_{31} &= K_{21}K_{32} - K_{22}K_{31}, \quad M_{32} = K_{12}K_{31} - K_{11}K_{32} \\ M_{33} &= K_{11}K_{22} - K_{12}K_{21} \\ |K| &= K_{11}K_{22}K_{33} - K_{11}K_{23}K_{32} - K_{12}K_{21}K_{33} + K_{12}K_{23}K_{31} \\ &\quad + K_{13}K_{21}K_{32} - K_{13}K_{22}K_{31} \end{aligned}$$

Formula (34) is a set of closed ordinary differential equations with initial values. These equations can be solved by the Gill or R-K methods.

III. The Flow on the Attachment Line

The numerical method used by Thompson [3] to solve the set of dominant equations for the turbulent boundary layer on the attachment line expressed $R_{\theta_{11}}$, n and Z_1 as the curvilinear or analytic formula of C^* and $M_{a.l}$. The formula used was

$$H_1 = (1 + 2n)/n \qquad (35)$$

and this could find θ_{11}, tgB and $\delta - \delta_1$ on the attachment line. Because u_1=tgB=0, that is $|K| = 0$ on the attachment line, therefore with the set of equations in (34) there is singularity on the attachment line. Because of this, calculations should begin from the downstream Δx area on the attachment line. In light of the fact that the flow on the attachment line is symmetrical, then

$$tg\beta = (d\theta_{11}/dx) = d(\delta - \delta_1)/dx = 0$$

Taking θ_{11}, tgβ and $\delta - \delta_1$ in the neighborhood of the attachment line in accordance with Tylor's expansion in series, we retained the first non-zero item and obtained the initial value in the Δx area

$$\left.\begin{aligned} &(\theta_{11})_{\Delta x} = (\theta_{11})_{a.l};\ (tg\beta)_{\Delta x} = \Delta x \cdot \left(\frac{d\,tg\beta}{dx}\right)_{a.l};\\ &(\delta - \delta_1)_{\Delta x} = (\delta - \delta_1)_{a.l} \end{aligned}\right\} \qquad (36)$$

The calculations in this paper which took $\Delta x = 0.005 c_n$, attained satisfactory results.

IV. The Process of Numerical Calculations and Calculation Examples

1. Based on the potential flow theory we calculated velocity distribution u_1 and span velocity v_1 outside the boundary layer on the normal profile of a yawed wing.

2. From the known $M_{a.l}$ and C* values along the attachment

line we calculated $(\theta_{11})_{a.l}$, $(dtg\beta/dx)_{a.l}$ and $(\delta - \delta_1)_{a.l}$ and then from formula (36) we calculated the above mentioned values of the downstream Δx area on the attachment line so as to solve the initial values of the set of equations.

3. We used the Gill (or R-K) method to carry out a numerical solution for the set of equations in (34) and finally we found the θ_{11}, $tg\beta$, $\delta - \delta_1$ as well as ε and the wall friction coefficient values on each nodal point along the X coordinate.

4. When we calculated $\beta + \varepsilon = 90^\circ$ (fig.2) there was separation.

Fig. 3 is Cumpsty and Head's experimental measurement results for the boundary layer of a yawed wing with a sweep-back angle of 60°.

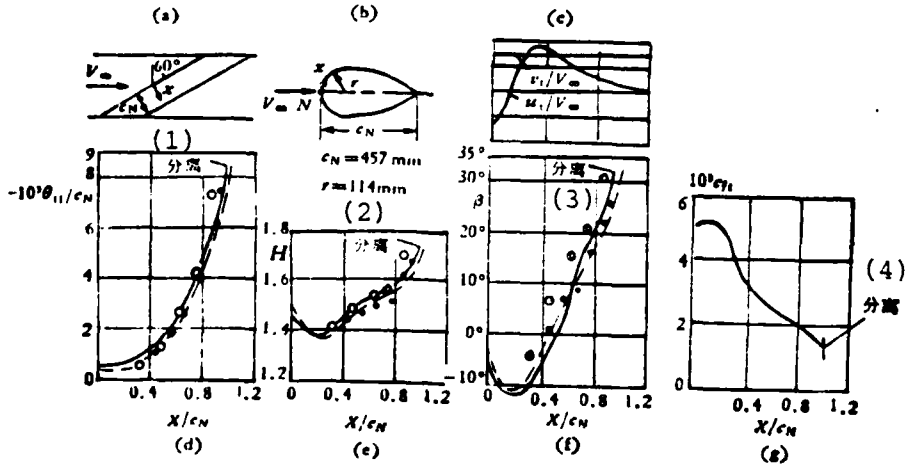

图 3

(5) ●.○ 两种不同边界层探针测量结果，——本文计算结果，———Redeker 计算结果，

(6) $Re = \frac{V_\infty c_N}{\nu} = 1.4 \cdot 10^6$，后缘坐标 $x = 1.2c_N$

Fig. 3

Key: 1. Separation
2. Separation
3. Separation
4. Separation

Fig. 3 (continued)

5. ●, 0 are the measurement results of two different types of boundary layers,——— indicates the calculation results of this paper, --- indicates Redeker's calculation results
6. $Re=\frac{V_\infty \, cn}{v}=1.4\cdot 10^6$, trailing edge coordinate trailing edge coordinate $x=1.2c_n$

Fig. (3a) is a sketch of an experimental installation, fig. (3b) is a normal wing profile, fig. (3c) is the measured velocity distribution on the wing surface, figs. (3d), (3e) and (3f) compare the values and measurement results of θ_{11}, H and β along x presented in this paper with the calculation results given by Redeker [1], fig. (3g) is this paper's calculated distribution value along x of the wall stream friction coefficient. We can see from this figure that the calculation results of this paper agree well with the experiment results. When compared with Redeker's calculation results, the results given in this paper for the area near the front of the separation line are even more identical to the experiment results. This paper calculated the separating point coordinate $X=1.004c_n$ (a little forward as compared to Redeker's results), $\beta=33.63^\circ$, H=1.755, $\theta_{11}=c_n\cdot 8.412\cdot 10^{-3}$. In the calculation examples, a layer stream recovery area did not appear (reference [10] mentions the possibility of a recovery area appearing under a very strong leading edge accelerating pressure gradient). This program was computed on a TQ-16 in approximately 25 minutes (including 101 dot output).

References

[1] Redeker, G.Z., Z. Flugwiss, 10(1973).

[2] Cumpsty, N.A., Head, M.R., Part I,II, Aeron. Quart. 18(1967).

[3] Thompson, B.G.J., MacDonald, A.G.J., ARC CP, 1307(1974).

[4] Ke Qin, H.E., Ji Bieli, N.A., Luo Si, Theoretical Hydromechanics. Vol. 1, Book 1, 32-45.

[5] Бай Ши-и. Турбулентное течение жидкостей и газов, 120—126.

[6] Lu Hanjiang, The Attached Layer Theory, 152-155.

[7] Heal, M.R., ARC R.& M., 3152(1958).

[8] Green, J.E., J.F.M., 31, Part IV(1968), 753-778.

[9] Cumpsty, N.A., Head, M.R., Part IV, Aeron. Quart. 21(1970).

[10] Thompson, B.G.J., ARC CP 1308(1974).

CALCULATION FOR THREE-DIMENTIONAL TURBULENT BOUNDARY LAYER ON A YAWED WING IN COMPRESSIBLE FLOW

Zhang Guofu

Abstract

This paper starts from the equations of motion in generalized curvilinear coordinates and the model of Head's two-dimensional entrainment theory, and derives a set of equations along surface curve on normal profile of a yawed wing for a compressible three-dimensional turbulent boundary layer. If there is a strong favourable pressure gradient in the neighbourhood of leading edge of the wing, divergence will arise in convertional methods. Therefore a typical form of a set of ordinary differential equations with initial values is obtained by matrix transformation in this paper. These equations have been solved by numerical computation.

Thompson and MacDonald's computational results on flow around an attachment line in the leading edge of a yawed wing have been used as the initial values to solve the set of ordinary differential equations.

The present method can be used to calculate the separation position of boundary layer, various boundary layer thicknesses and wall stress, and describe the difference between streamlines outside boundary layer and streamlines on the wall.

Typical computational shows that the present method agrees well with experiment results.

ON THE RAYLEIGH-TAYLOR INSTABILITY OF A CURRENT SHEET IN AN ELECTROMAGNETICALLY DRIVEN SHOCK WAVE APPARATUS

by Xu Fu
(Institute of Mechanics, Academia Sinica)

1. Current in Shock Wave Apparatus

At present, we will consider the electromagnetically driven shock wave apparatus as shown in fig. 1. After discharge, a very strong shock wave is propagated towards the right, the rear surface is a current layer and it separates the plasma and magnetic field. In 1959, Wright and Black [1] researched in detail the current in an electromagnetically driven shock wave apparatus during the initial period of discharge. After assuming that current i and time t form a direct ratio, they found a similar solution. At the same time, the current layer used iso-acceleration to move towards the right side and it could be predicted that this would produce Rayleigh-Taylor instability. Because acceleration a was large, the instability growth rate w was also very large.

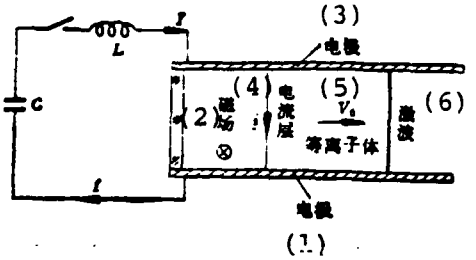

Fig. 1

Fig. 1

Key: 1. Electrode
2. Magnetic field
3. Electrode
4. Current layer
5. Plasma
6. Shock wave

We let the current sheet use iso-acceleration a to move towards the right (see fig. 2)

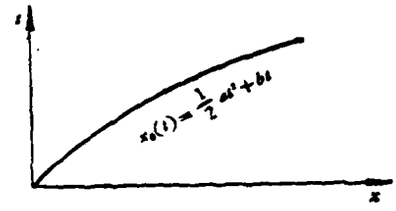

Fig. 2

Coordinate $x_o(t)$ and velocity $v_o(t)$ of the curr ent sheet are separately

$$\left.\begin{aligned} x_0(t) &= \frac{1}{2}at^2 + bt \\ v_0(t) &= at + b \end{aligned}\right\} \qquad (1)$$

Given that the plasma is compressible, non-viscous and non-heat conducting, the electric conduction rate is $\sigma = \infty$, and the magnetic conduction rate is $\mu = 1$. Using Gauss units, then the fundamental equations are:

$$\left.\begin{aligned} &\frac{\partial \boldsymbol{H}}{\partial t} = \nabla \times (\boldsymbol{V} \times \boldsymbol{H}) \\ &\nabla \cdot \boldsymbol{H} = 0 \\ &\rho\left\{\frac{\partial \boldsymbol{V}}{\partial t} + (\boldsymbol{V}\cdot\nabla)\boldsymbol{V}\right\} = -\nabla p - \frac{1}{4\pi}\boldsymbol{H}\times(\nabla\times\boldsymbol{H}) \\ &\frac{\partial \rho}{\partial t} + (\boldsymbol{V}\cdot\nabla)\rho + \rho\nabla\cdot\boldsymbol{V} = 0 \\ &\frac{\partial p}{\partial t} + (\boldsymbol{V}\cdot\nabla)p = \gamma\frac{p}{\rho}\left\{\frac{\partial \rho}{\partial t} + (\boldsymbol{V}\cdot\nabla)\rho\right\} \end{aligned}\right\} \qquad (2)$$

The kinematic bound conditions on the current sheet are:
On $x=x_o(t)$

$$\left.\begin{aligned} N &= \boldsymbol{V}\cdot\boldsymbol{n} \\ \frac{d\boldsymbol{n}}{dt} &= \boldsymbol{n}\times(\boldsymbol{n}\times\nabla\boldsymbol{V})\cdot\boldsymbol{n} \end{aligned}\right\} \qquad (3)$$

In formulas (2) and (3), the symbols are the same as those used in common MHD books: γ is the gas - heat ratio, N is the current sheet's motion velocity, and n is the current sheet's normal direction.

The kinematic boundary conditions on the current sheet can be attained from the set of equations in (2) by carrying out integration on the current sheet:

$$\left.\begin{aligned} &[(\boldsymbol{n}\cdot\boldsymbol{V}-N)\boldsymbol{H}]=0 \\ &\boldsymbol{n}\cdot[\boldsymbol{H}]=0 \\ &-\boldsymbol{n}[p]-\rho(\boldsymbol{n}\cdot\boldsymbol{V}-N)[\boldsymbol{V}]+\frac{1}{4\pi}\{\boldsymbol{n}\times[\boldsymbol{H}]\times\underline{\boldsymbol{H}}\}=0 \\ &[\rho(\boldsymbol{n}\cdot\boldsymbol{V}-N)]=0 \end{aligned}\right\} \qquad (4)$$

In the formula, the brackets indicate the difference in the physical quantity of the two sides of the current sheet. $\underline{H}$ indicates the arithmetic mean of H on the two sides of the current sheet.

We assume that

$$\left.\begin{aligned} &p=p_{00}e^{-K(z-z_0(t))}, \qquad \rho=\rho_{00}e^{-K(z-z_0(t))} \\ &\boldsymbol{V}=\boldsymbol{V}_0=(at+b)\boldsymbol{i}, \quad H_2^0=H_2^0\boldsymbol{K} \end{aligned}\right\} \qquad (5)$$

In the formula, $h=\frac{\rho_0 a^2}{p_0}$, p_o and ρ_o indicate the pressure and density of the plasma on the current sheet, i and K are the unit vectors of the x and z directions, H_1^0 is the added magnetic field, and H_2^0=a constant. It is very easy to test and verify that formula (5) satisfies the set of equations in (2).

Taking formula (5) as the basic current, it agrees very well with the Wright-Black solution [1] in the vicinity of the current sheet.

The magnetic field on the left side of the current sheet is

$$H_1 = H_1^0 j \qquad (6)$$

In the formula, H_1^0=a constant. j is the unit vector of the y direction.

In order for the boundary conditions of (4) to be satisfied, there must be

$$\frac{(H_1^0)^2}{8\pi} = p_0 + \frac{(H_1^0)^2}{8\pi}. \qquad (7)$$

For convenience of discussion, below we will take a coordinate system on the current sheet.

2. Equations and Boundary Conditions of Small Disturbances

We superposed a small disturbance on the basic current of the plasma and magnetic field. We assume that all of the disturbance quantity $\tilde{f}$ are shaped like

$$\tilde{f} = f(x)e^{\omega t + iK_y y + iK_z z}$$

In the formula, K_y and K_z are wave numbers. We can then finally obtain an equation which satisfies the disturbance quantity $\tilde{v}_x$ in the plasma:

$$\frac{d^2\tilde{v}_z}{dx^2} - \left\{ \frac{\gamma p_0^2 a\omega^2}{\gamma p_0\rho_0\omega^2 + \frac{(H_1^0)^2}{4\pi} e^{hz}(\rho_0\omega^2 + \gamma p_0 K_z^2)} \right.$$

$$+ \left((\rho_0\omega^2)^2 K_y^2 \frac{(H_1^0)^2}{4\pi} \cdot e^{hz} \cdot h \right) \Big/ \left\{ \left(\rho_0\omega^2 + \frac{(H_1^0)^2}{4\pi} e^{hz} K_z^2 \right) \left[(\rho_0\omega^2) + (K_y^2 + K_z^2) \right.\right.$$

$$\left.\left. \times \left(\gamma p_0\rho_0\omega^2 + \frac{(H_1^0)^2}{4\pi} e^{hz}(\rho_0\omega^2 + \gamma p_0 K_z^2) \right) \right] \right\} \left. \right\} \frac{d\tilde{v}_z}{dx}$$

$$- \left\{ K_y^2 + K_z^2 + \frac{(\rho_0\omega^2)^2}{\gamma p_0\rho_0\omega^2 + \frac{(H_1^0)^2}{4\pi} e^{hz}(\rho_0\omega^2 + \gamma p_0 K_z^2)} \right.$$

$$+ \frac{(\gamma - 1)(\rho_0 a)^2 (K_y^2 + K_z^2)}{\gamma p_0\rho_0\omega^2 + \frac{(H_1^0)^2}{4\pi} e^{hz}(\rho_0\omega^2 + \gamma p_0 K_z^2)} - \left(p_0 a \rho_0\omega^2 K_y^2 (K_y^2 + K_z^2) \frac{(H_1^0)^2}{4\pi} e^{hz} \right.$$

$$\left. \cdot h \right) \Big/ \left\{ \left(\rho_0\omega^2 + \frac{(H_1^0)^2}{4\pi} e^{hz} K_z^2 \right) \left[(\rho_0\omega^2)^2 + (K_y^2 + K_z^2) \left(\gamma p_0\rho_0\omega^2 \right.\right.\right.$$

$$\left.\left.\left. + \frac{(H_1^0)^2}{4\pi} e^{hz}(\rho_0\omega^2 + \gamma p_0 K_z^2) \right) \right] \right\} \left. \right\} \tilde{v}_z = 0 \qquad (8)$$

After finding $\tilde{v}_x$, $\tilde{v}_y$ and $\tilde{v}_z$ can be found from the following formulas:

$$\tilde{v}_y = - \frac{\left\{ \gamma p_0\rho_0\omega^2 + \frac{(H_1^0)^2}{4\pi} e^{hz}(\rho_0\omega^2 + \gamma p_0 K_z^2) \right\} iK_y \frac{d\tilde{v}_z}{dx} - \rho_0^2 a\omega^2 iK_y \tilde{v}_z}{(\rho_0\omega^2)^2 + (K_y^2 + K_z^2) \left\{ \gamma p_0\rho_0\omega^2 + \frac{(H_1^0)^2}{4\pi} e^{hz}(\rho_0\omega^2 + \gamma p_0 K_z^2) \right\}} \qquad (9)$$

$$\tilde{v}_x = - \frac{\gamma p_0 \left\{ \rho_0\omega^2 + \frac{(H_1^0)^2}{4\pi} e^{hz} K_z^2 \right\} iK_z \frac{d\tilde{v}_z}{dx} - \rho_0 a iK_z \left\{ \rho_0\omega^2 + \frac{(H_1^0)^2}{4\pi} e^{hz}(K_y^2 + K_z^2) \right\} \tilde{v}_z}{(\rho_0\omega^2)^2 + (K_y^2 + K_z^2) \left\{ \gamma p_0\rho_0\omega^2 + \frac{(H_1^0)^2}{4\pi} e^{hz}(\rho_0\omega^2 + \gamma p_0 K_z^2) \right\}} \qquad (10)$$

Each of the other quantities can also be found from the disturbance equation.

Now, we will find a solution for the disturbance magnetic field on the left side of the current sheet.

The disturbance magnetic field has potential and therefore

$$\tilde{H}_1 = \nabla\varphi \tag{11}$$

The flux conservation of the disturbance magnetic field is given as

$$\nabla^2\varphi = 0 \tag{12}$$

can be written as

$$\varphi = \varphi_0 \cdot e^{K_1 x} \cdot e^{\omega t + iK_y y + iK_z z}, \quad K_1^2 = K_y^2 + K_z^2, \tag{13}$$

When substituted into formula (11), we can find $\tilde{H}_1$.

For the linearization of the kinetic boundary conditions of (4) and the kinematic boundary conditions of (3) needed to fulfill the current sheet x=0, after eliminating each disturbance quantity, we could obtain the $\tilde{v}_x$ conditions needed to fulfill x=0:

$$\left(\rho_{1}\omega^2 + \frac{(H_1^0)^2}{4\pi} K_z^2\right)\left\{\gamma p_0\rho_0\omega^2 + \frac{(H_1^0)^2}{4\pi}(\rho_0\omega^2 + \gamma p_0 K_z^2)\right\}\frac{d\tilde{v}_x}{dx}\Big|_{x=0} + \rho_0\omega\left\{\left[\rho_1\omega^2 + \frac{(H_1^0)^2}{4\pi} K_z^2\right]\gamma p_0 K_z^2 + K_y^2\left[\gamma p_1\rho_0\omega^2 + \frac{(H_1^0)^2}{4\pi}(\rho_0\omega^2 + \gamma p_0 K_z^2)\right]\right\}\tilde{v}_x\Big|_{x=0} - \frac{(H_1^0)^2}{4\pi}\frac{K_y^2}{K_1}\left\{(\rho_0\omega^2)^2 + (K_y^2 + K_z^2)\left[\gamma p_0\rho_0\omega^2 + \frac{(H_1^0)^2}{4\pi}(\rho_1\omega^2 + \gamma p_0 K_z^2)\right]\right\}\tilde{v}_x\Big|_{x=0} \tag{14}$$

Another natural boundary condition is

When $x \longrightarrow +\infty$, $\tilde{v}_x$ is limited (15)

3. The Magnetic Field is Absent from the Plasma ($H_2^0=0$)

When $H_2^0=0$ is substituted into formula (8), formula (8) is transformed into a constant coefficient divalent ordinary differential equation and its solution is

$$\tilde{v}_x = ce^{-K_2 x} \quad K_2 > 0 \tag{16}$$

The the K_2 found from the equation should be satisfactory

$$K_2^2 + hK_2 - (K_y^2 + K_z^2) - \frac{\rho_0\omega^2}{\gamma p_0} - \frac{\gamma - 1}{\gamma}\frac{ha}{\omega^2}(K_y^2 + K_z^2) = 0 \tag{17}$$

The dispersion equation is obtained from the boundary conditions of (14):

$$\rho_0\omega^2 + \frac{(H_1^0)^2}{4\pi}\frac{K_y^2}{K_1}K_2 + \frac{\gamma - 1}{\gamma}h\frac{(H_1^0)^2}{4\pi}\frac{K_y^2}{K_1} - \rho_0 a K_2 = 0 \tag{18}$$

Note that the boundary conditions of (15) have already been fulfilled.

Equation (18) shows that acceleration a causes the current sheet to be unstable and the greater a is, the greater ω is. If a is changed to a negative sign, then $\omega^2 < 0$, and the motion is stable. Magnetic field H_1^0 causes a stable effect.

If there is only disturbance in the z direction, we can find:

$$\omega^2 = aK_z \qquad (19)$$

In most situations, if $K_z > K_y$, we approximately take $\omega^2 = aK_2$ in formula (18), and we substitute it into formula (17)

$$K_1 = \sqrt{K_y^2 + K_z^2} \qquad (20)$$

Further, when substituted into formula (18), then

$$\omega^2 = a\sqrt{K_y^2 + K_z^2} - 2\frac{\rho_0}{\rho_0}K_y^2 - 2\frac{\gamma - 1}{\gamma}aK_y^2/\sqrt{K_y^2 + K_z^2} \qquad (21)$$

Some works [2-4] have studied the Rayleigh-Taylor instability in its experimental aspect. Results have shown that formula (19) qualitatively agrees with the experiments.

4. The Magnetic Field is Present in the Plasma ($H_2^0 \neq 0$)

Kruskal and Schwarzschild [5] have computed a similar problem. They assumed that hx was very small and then transformed equation (10) into a constant coefficient. This cannot be done in an electromagnetically driven shock wave apparatus.

If our aim is only to find the dispersion relationship, then from formula (14) we can see that it is only necessary to correctly find the value of $\frac{d\tilde{v}_x}{dx}/\tilde{v}_x$ in x=0.

Equation (10) is written as

$$\frac{d^2\tilde{v}_x}{dx^2} + A(x)\frac{d\tilde{v}_x}{dx} + B(x)\tilde{v}_x = 0 \qquad (22)$$

Letting

$$f = \frac{d\tilde{v}_x}{dx} \Big/ \tilde{v}_x,$$

then

$$\frac{df}{dx} + f^2 + A(x)f + B(x) = 0 \qquad (23)$$

When $x \longrightarrow +\infty$, formula (10) is

$$\frac{d^2\tilde{v}_x}{dx^2} - (K_y^2 + K_z^2)\tilde{v}_x = 0 \qquad (24)$$

Therefore

$$\text{when } x \longrightarrow +\infty \ , \ f(x) = -\sqrt{K_y^2 + K_z^2} \qquad (25)$$

When x is relatively large, f(x) changes slowly and therefore the conditions in (25) can be approximately changed to

$$\text{when } x = \frac{1}{h}, \ f(x) = \sqrt{K_y^2 + K_x^2} \qquad (26)$$

Now, we use an approximation method of equation (23) to solve and fulfill formula (26).

If

$$A(x) = A_0 + A_1(x) \quad B(x) = B_0 + B_1(x) \qquad (27)$$

in the neighborhood of x=0, it is assumed that

$$f(x) = -K_0 + f_1(x) \qquad (28)$$

In formulas (27) and (28), K_o is a positive constant, and A_1,

B_1 and f_1 are first order small quantities. After being substituted into formula (23)

$$K_0^2 - A_0 K_0 + B_0 = 0 \tag{29}$$

and

$$\frac{df_1}{dx} + (A_0 - 2K_0)f_1 + B_1(x) - K_0 A_1(x) = 0 \tag{30}$$

The conditions which satisfy $f_1(x)$ are

$$f_1(x) = K_0 - \sqrt{K_y^2 + K_z^2} \quad \text{当 } x = \frac{1}{h} \tag{31}$$

After solving $f_1(x)$, we can find

$$f(x)\Big|_{x=0} = \frac{\frac{d\tilde{v}_x}{dx}}{\tilde{v}_x}\Big|_{x=0}$$

$$= -K_0 + e^{\frac{A_0 - 2K_0}{h}} \cdot \left\{K_0 - \sqrt{K_y^2 + K_z^2} + \int_0^{\frac{1}{h}} (B_1(x) - K_0 A_1(x))dx\right\} \tag{32}$$

Substituted into formula (14), we then obtain the dispersion relationship.

If we approximately take $f(x)\big|_{x=0} = -K_o$, then the dispersion relationship is

$$\rho_{0i}\omega^2 + \frac{(H_1^0)^2}{4\pi} K_x^2 + \frac{(H_1^0)^2}{4\pi} \frac{K_y^2}{K_1} - \rho_{0i} a K_0 + \Big((\gamma - 1)\rho_{0i} a\omega^2 \times \frac{(H_1^0)^2}{4\pi} \frac{K_y^2}{K_1}$$
$$+ (\gamma - 1)(\rho_{0i} a)^2 \frac{(H_1^0)^2}{4\pi} K_z^2 \Big) \Big/ \Big(\gamma p_{0i}\rho_{0i}\omega^2 + \frac{(H_1^0)^2}{4\pi} (\rho_{0i}\omega^2 + \gamma p_0 K_z^2) \Big)$$
$$- \Big\{ - \Big[\gamma p_{0i}\rho_{0i}\omega^2 + \frac{(H_1^0)^2}{4\pi} (\rho_{0i}\omega^2 + \gamma p_0 K_z^2) \Big] \Big\{ \Big[(\rho_{0i}\omega^2)^2 K_z^2 \frac{(H_1^0)^2}{4\pi} h \Big] K_0$$
$$- \rho_{0i}^2 a\omega^2 K_y^2 (K_y^2 + K_z^2) \frac{(H_1^0)^2}{4\pi} h \Big\} \Big\} \Big/ \Big\{ (\rho_{0i}\omega^2)^2 + (K_y^2 + K_z^2) \Big[\gamma p_{0i}\rho_{0i}\omega^2$$
$$+ \frac{(H_1^0)^2}{4\pi} (\rho_{0i}\omega^2 + \gamma p_0 K_z^2) \Big] \Big\} \qquad (33)$$

Using this formula, we can compute the size of the magnetic field required to eliminate Rayleigh-Taylor instability. The direction of the magnetic field H_2^0 is K and this can prevent z direction motion. Because of this, if K_y=0, the above formula changes to

$$\rho_{0i}\omega^2 + \frac{(H_1^0)^2}{4\pi} K_z^2 - \rho_{0i} a K_0 + \frac{(\gamma - 1)(\rho_{0i} a)^2 \frac{(H_1^0)^2}{4\pi} K_z^2}{\gamma p_{0i}\rho_{0i}\omega^2 + \frac{(H_1^0)^2}{4\pi} (\rho_{0i}\omega^2 + \gamma p_0 K_z^2)} = 0 \qquad (34)$$

Now, letting ω^2=0, the derived K_o is

$$\frac{(H_1^0)^2}{4\pi} K_z^2 + \frac{\gamma - 1}{\gamma} \frac{(\rho_{0i} a)^2}{p_0} - \rho_{0i} a K_0 = 0 \qquad (35)$$

In formula (29), letting ω^2=0, the derived K_o is

$$K_0 = K_z \cdot \sqrt{1 + \frac{\gamma - 1}{\gamma} \frac{h^2}{K_z^2} \frac{p_0}{(H_1^0)^2} 4\pi} \qquad (36)$$

After being substituted into (35) and simplified, we then have

$$2 \times \frac{(H_1^0)^2}{8\pi p_0} \cdot \sqrt{1 + \frac{\gamma - 1}{2\gamma} \left(\frac{h}{K_z} \right)^2 \cdot \frac{p_0 \cdot 8\pi}{(H_1^0)^2}} - \frac{h}{K_z} = 0 \qquad (37)$$

Fig. 3 is the curve of $\frac{1}{p_o}\frac{(H_2^0)^2}{8\pi}$ and $\frac{h}{K_z}$. Results show that for a disturbance in any z direction to be able to become stable it is only necessary for

$$\frac{1}{p_0}\frac{(H_2^0)^2}{8\pi} > \frac{\gamma}{\gamma-1} \tag{38}$$

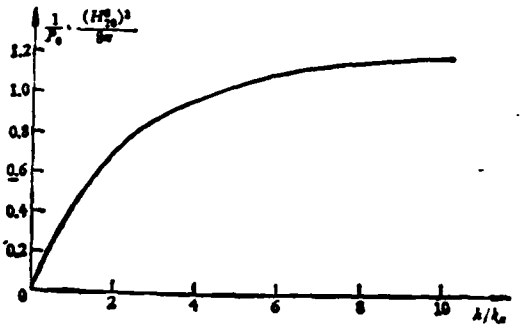

Fig. 3

References

[1] Wright, J.K., Black, M.C., A theory of electromagnetically driven shock waves, J. Fluid Mech. 6, Part 2(1959), 289-301.

[2] Dickinson, H., et.al., Observation of apparent flute type plasma instabilities, Phys. Fluids, 3, 3(1960), 480-481.

[3] Curzon, F.L., et.al., Experiments on the growth rate of surface instabilities in a linear pinched discharge, Proc. Roy. Soc., 257(1960), 386-401.

[4] Albares, D.J., et.al., Rayleigh-Taylor instabilities in a stabilized linear pinch tube, Phys. Fluids, 4,8(1961), 1031-36.

[5] Kruskal, M., Schwarzachild, M., Some instabilities of a completely ionized plasma, Proc. Roy. Soc.,223(1954),348-360.

MEASUREMENT OF ELECTRON DENSITY BEHIND A STRONG SHOCK WAVE USING 3 cm MICROWAVE TRANSMISSION

by Zhu Naiyi and Li Xuefen
(Institute of Mechanics, Academia Sinica)

Abstract

This article presents the working principle of a 3 cm microwave transmission method. It was used to measure the electron density behind strong shock waves in an 800 mm diameter shock tube. The variation of electron density with M number is obtained, and it is in good agreement with other measurement data, and is also in good agreement with theoretical predictions.

I. Testing Apparatus

Two split glass windows are installed on the test sections of an 800 mm diameter shock wave tube [1]. The surface in the glass and the wall inside the shock wave tube is flat so that there was no serious disturbance of the gas produced. A continuous iso-amplitude microwave signal is transmitted through a horn antenna direction after 300KC square modulation. From the level of the split window opening it goes through the shock wave tube and is then received by the receiving antenna. In order to eliminate the strong electromagnetic field interference caused in the shock wave motion process, we floated the entire receiving system and used a symmetrical output circuit to transmit the signal from the detector to the oscilloscope.

II. Working Principle

Microwave transmission is used to measure the electron

density of plasma in shock waves based on the relative changes of the microwave power behind the shock wave tube. The differences between the shock waves reaching in front and behind are manifested in two major areas. The first is before the shock waves reach the window opening. The microwave interface has weak reflection (similar in the areas of the two window openings) between the surface inside the glass window and the vacuum. When the shock waves reach the opening, the microwave interface area has relatively strong reflection (when the electron density of the plasma is different so is the strength of the reflection) in between the surface inside the glass and the plasma. The second area is before the shock waves reach. When the microwaves go through a shock wave tube which has an 800 mm long free space internal area, there is "background" power attenuation. When the shock waves reach, they penetrate through the 800 mm plasma and can produce an added power attenuation. Based mainly on this added power attenuation we determined the electron density value in the shock wave.

1. Reflection of the Surface Area in the Window Opening

The reflectivity of the microwave on the 1 medium to 2 medium reflection surface [2] is

$$\tilde{\rho}_{1,2} = \frac{\tilde{z}_{w_2} - \tilde{z}_{w_1}}{\tilde{z}_{w_2} + \tilde{z}_{w_1}} \qquad (1)$$

It is interrelated with the impedance of the medium wave on the two sides of the reflection surface

$$\tilde{z}_w = \sqrt{\frac{\mu\mu_0}{\tilde{\varepsilon}\tilde{\varepsilon}_0}} \qquad (2)$$

Under our conditions, the medium's magnetic conduction rate was usually $\mu \approx \mu_0$. For this reason

$$\tilde{\rho}_{1,2} = \frac{\tilde{\varepsilon}_1^{1/2} - \tilde{\varepsilon}_2^{1/2}}{\tilde{\varepsilon}_1^{1/2} + \tilde{\varepsilon}_2^{1/2}} \qquad (3)$$

The relative dielectric constant $\tilde{\varepsilon}/\varepsilon 0$ of the medium can be written as

$$(\tilde{\varepsilon}/\varepsilon_0)^{1/2} = n - j\chi \qquad (4)$$

In this formula, n is the common refractive index and $\chi = \frac{c}{\omega}a$ is the attenuation index. c is the velocity of light, ω is the microwave angular frequency, and a is the attenuation coefficient.

The reflective index of the two medium interface area microwaves, calculated on the basis of power, is

$$r_{1,2} = |\tilde{\rho}_{1,2}|^2 = \frac{(n_1 - n_2)^2 + (\chi_1 - \chi_2)^2}{(n_1 + n_2)^2 + (\chi_1 + \chi_2)^2} \qquad (5)$$

Because the inner diameter of the shock wave tube is far larger than the wave length of the microwave, the electron density in the shock wave is close to homogeneous. Given that the electromagnetic wave is transmitted in infinitely large, homogeneous Lorentz plasma, we can attain the n refractive index and χ attenuation index as follows

$$n = \left\{\frac{1}{2}\left(1 - \frac{\omega_p^2}{\omega^2 + \nu^2}\right) + \frac{1}{2}\left[\left(1 - \frac{\omega_p^2}{\omega^2 + \nu^2}\right)^2 + \left(\frac{\omega_p^2}{\omega^2 + \nu^2} \cdot \frac{\nu}{\omega}\right)^2\right]^{\frac{1}{2}}\right\}^{1/2} \quad (6)$$

$$\chi = \left\{-\frac{1}{2}\left(1 - \frac{\omega_p^2}{\omega^2 + \nu^2}\right) + \frac{1}{2}\left[\left(1 - \frac{\omega_p^2}{\omega^2 + \nu^2}\right)^2 + \left(\frac{\omega_p^2}{\omega^2 + \nu^2} \cdot \frac{\nu}{\omega}\right)^2\right]^{1/2}\right\}^{1/2} \quad (7)$$

In these formulas, ω_p is the characteristic frequency, and v is the collision frequency of electrons in the plasma

$$\nu = \left(\frac{8KT}{\pi m_e}\right)^{1/2} \cdot (N_i \cdot Q_{ei} + N_n \cdot Q_{en}) \quad (8)$$

Q_{ei} and Q_{en} are separately the electrons and ions, and the neutral particle collision section. In the working conditions of this article, $v=10^8$, $\omega=10^{10}$, that is $\omega \gg v$. Generally speaking, the effects of v can be disregarded.

2. The Attenuation of the Microwaves Penetrating Through the Plasma

As previously mentioned, in the working conditions of this article, we can regard an angular frequency as a plane electromagnetic wave propagated in an infinitely large medium:

$$A = A_0 \exp(j\omega t - \vec{\gamma} \cdot L) \quad (9)$$

In this formula, the transmission constant is

$$\vec{\gamma} = \alpha + j\beta \quad (10)$$

a is the attenuation coefficient, β is the phase constant, L=800 mm is the distance traveled by the microwave. When $v \ll \omega$

$$\alpha = \frac{\omega}{2c}\left[\left(\frac{\omega_p^2}{\omega^2}\right) \cdot \nu/\omega \cdot \sqrt{1 - \left(\frac{\omega_p^2}{\omega^2}\right)}\right] = \frac{\nu}{2c}\left[\left(\frac{n_e}{n_m}\right)\Big/\sqrt{1 - \frac{n_e}{n_m}}\right] \quad (11)$$

In the formula, $n_{ec}=m_c\omega^2/4\pi e^2$ is the cut-off density of the microwave, and n_e is the electron density in the plasma.

Based on the total attenuation of the microwave power after going through plasma, we deducted the effects of interface reflection and found attenuation coefficient a. Proceeding to the next step, we obtained electron density n_e.

III. Conclusion

The working frequency of the microwave transmission employed in this article is f=8.87Gc and the corresponding cut-off density is $n_{ec}\approx 1\times10^{12}/cm^3$.

In the 800 mm diameter shock wave tube presented in fig. 1, when $P_1=1\times10^{-2}$mmHg, under several types of M numbers, there is typical recording of 3cm microwave transmission. When M_s is approximately equal to 12.5, absorption cannot be seen; when M_s is approximately equal to 13.5, weak absorption begins; when M_s is approximately equal to 16, absorption is about one-half; when M_s is approximately equal to 17.6, cut-off begins to appear; when M_s is approximately equal to 20, there is relatively long time cut-off.

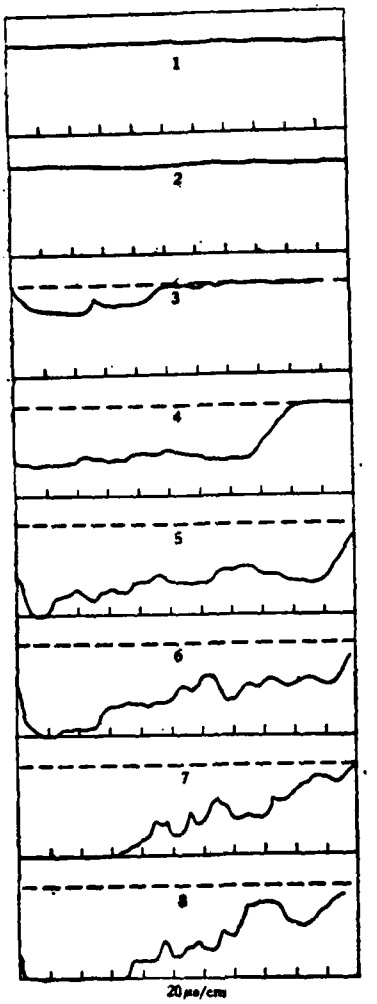

图 1 $P_1 = 1\times10^{-2}$mmHg, 3cm 透射仪记录

$f = 8.87$Gc

(1) 1 M, = 12.5 看不出吸收.
(2) 2 M, = 13.5 有弱吸收
(3) 3 M, = 14.2 有部分吸收.
(4) 4 M, = 16 吸收约一半
(5) 5 M, = 17.6 开始有截止.
(6) 6 M, = 18.7 部分截止
(7) 7 M, = 19.9 较长时间截止.
(8) 8 M, = 20.5 较长时间截止

Fig. 1 When $P_1=1x10^{-2}$mmHg, the 3 cm Transmission Record
f=8.87Gc

Key: 1. M_s=12.5 invisible absorption
2. M_s=13.5 weak absorption
3. M_s=14.2 partial absorption
4. M_s=16 absorption about one-half
5. M_s=17.6 cut-off begins
6. M_s=18.7 partial cut-off
7. M_s=19.9 relatively long time cut-off
8. M_s=20.5 relatively long time cut-off

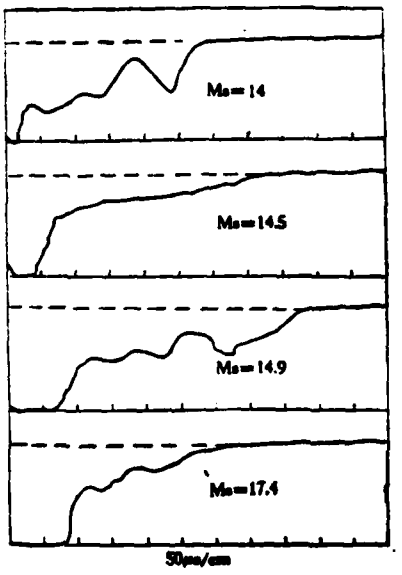

Fig. 2 When $P_1=1x10^{-1}$mmHg, the 3cm Transmission Record
f=8.87Gc

Test measurement attenuation coefficient a given in table 1 changes with the M number. Proceeding to the next step, we can attain electron density n_e behind the shock wave which follows

the change relation of the M number (see fig. 3).

M_s	13.5	14.2	15.9	16	17.2	17.6
(1) α(奈培/米)	0.03	0.17	0.36	0.50	0.50	≥3

Table 1 Attenuation Coefficient a Changes With the M Number ($P_1=1x10^{-2}$mmHg)

Key: 1. a (neper/meter)

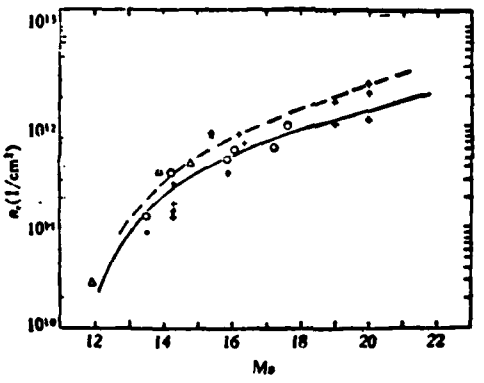

Fig. 3 The Electron Density of the Air Behind the Shock Wave $P_1=1x10^{-2}$mmHg

--- Gilmore [4], —— Soviet Union's Academy of Sciences, + Zhu Naiyi [3], O 3cm transmission, Δ 3cm interferometer, ● 8mm transmission

Within the $P_1=1x10^{-2}$mmHg given in fig. 3, when M_s=12-22, this is the peak value of the air's electron density behind the shock wave. The measurement results in this article, which used

3cm microwave transmission, are not only identical with near free molecule Langmuir probe measurements but are also in good agreement with the reference values presented for the 3cm microwave interferometer and the 8mm microwave transmission. The test measurement values were relatively close to the equilibrium values which were theoretically predicted.

Comrades Luo Jun, Li Shuqin and Li Lianxiang participated in part of the testing work for this article. Comrades Ye Youzhang and Gao Lingzhi gave enthusiastic aid in related work for this article and here we would like to express our gratitude to them.

References

[1] Zhu Naiyi, Li Hongde, Zou Huiliang and Li Lianxiang, Mechanics, 3(1978), 234.

[2] Heald, M.A., Wharton, C.B., Plasma diagnostics with microwaves, John Wiley and Sons, New York(1965).

[3] Zhu Naiyi and Li Lianxiang, Study of the Near Free Molecule Flow Langmuir Probe and Ionization Shock Wave Structure.

[4] Gilmore, F.R., RM-1543(1955).

[5] Предводителев, А. С., Ступоченко, Е. В., Таблицы Термодинамических Функций Воздуха (1962).

MEASUREMENT OF ELECTRON DENSITY BEHIND A STRONG SHOCK WAVE USING 3 cm MICROWAVE TRANSMISSION

Zhu Naiyi Li Xuefen

(Institute of Mechanics, Academia Sinica)

Abstract

This article presents the working principle of a 3 cm microwave transmission method. It was used to measure the electron density behind strong shock waves in an 800 mm dia. shock-tube. The variation of electron density with Ms is obtained, and it is in good agreement with the data from Langmuir probe measurements, and is also in good agreement with theoretical predictions.

1. The Non-Linear Interference Factor

Based on Nielsen's [1] proposal, the wing-body combination force can be viewed as a combination of each component's normal force and interference quantity

$$C_{N_{(B+WB)}} = C_{N_B} + \{K_{W(B)P} + K_{B(W)P}\} C^{\alpha}_{N_W} \alpha \frac{S_W}{S_B} \qquad (1)$$

In the formula, $K_{W(B)P}$ and $K_{B(W)P}$ are separately the interference factors of the wing when there is a body, and the wing's induced lift of the body. The lower sign P indicates the quantity of the linear system. $K_{W(B)P}$ and $K_{B(W)P}$ are identical [1].

Based on the "leading edge suction analogy" theory, the normal lift of a single wing is equal to [5]

$$C_{N_W} = C^{\alpha}_{N_W} \sin\alpha\cos\alpha + (\tilde{K}_{VLE} + \tilde{K}_{VSE})\sin^2\alpha \qquad (2)$$

$$\tilde{K}_{VLE} = C^{\alpha}_{N_W}\left(1 - \frac{C^{\alpha}_{N_W}}{\pi A}\right) \Big/ \cos\Lambda$$

$$\tilde{K}_{VSE} = 2\left(\frac{c_s}{s_m}\right)\frac{(C^{\alpha}_{N_W})^2}{\pi A}.$$

In the formula, $\tilde{K}_{VLE}$ and $\tilde{K}_{VSE}$ are separately the leading edge vortex and side edge vortex lift derivatives. If we assume that the "suction analogy" theory is also applicable to the wing-body combination, then at this time it is necessary to come forth with more non-linear interference factors

$$C_{N_{(B+WB)}} = C_{N_B} + \{(K_{W(B)P} + K_{B(W)P})C^{\alpha}_{N_W}\sin\alpha\cos\alpha + (K_{W(B),VLE} + K_{B(W),VLE})\tilde{K}_{VLE}\sin^2\alpha + (K_{W(B),VSE} + K_{B(W),VSE})\tilde{K}_{VSE}\sin^2\alpha\}\frac{S_W}{S_B} \qquad (3)$$

In this formula, the definitions of each non-linear interference

THE INTERFERENCE FACTOR OF VORTEX LIFT OF WING-BODY COMBINATIONS AT SUPERSONIC SPEED

by Yin Xieyuan
(University of Science and Technology of China, Department of Mechanics)

During the 1950's, Nielsen and others proposed the concept of "interference factors" (reference [1]) to compute the aerodynamic interference among wing-body combination components. Their method has become the basis for presently commonly used engineering computation methods. During the 1960's, comrade Ji Chuchun and others synthesized and developed the work of Nielsen [1] and Lebedev [2] and brought forth a set of computation handbooks [3] which have expanded the knowledge of and been widely used by aerodynamic design workers. Yet, what Nielsen presented was linearized lift "interference factors" which are suitable for the small attack angle range. At present, there is still no ready method which can be followed for the medium to large attack angle range because there is interference produced within the non-linear lift by body vortex and wing vortex. Although, very recently, Nielsen [4] brought forth the concept of the non-linear interference factor, yet he still used a numerical solution and this does not give a concrete computation method for the interference factor. Other authors have brought forth computation methods for wing-body combination attack angles but most also use numerical methods. Based on the "leading edge suction analogy" and "upwash theory", this article brings forth a computation theory for the non-linear interference factor and obtains corresponding formulas and curves. It can expand the application range of the current handbooks and is convenient for use in design departments.

1. The Non-Linear Interference Factor

Based on Nielsen's [1] proposal, the wing-body combination force can be viewed as a combination of each component's normal force and interference quantity

$$C_{N_{(B+WB)}} = C_{N_B} + \{K_{W(B)P} + K_{B(W)P}\} C^{\alpha}_{N_W} \alpha \frac{S_W}{S_B} \qquad (1)$$

In the formula, $K_{W(B)P}$ and $K_{B(W)P}$ are separately the interference factors of the wing when there is a body, and the wing's induced lift of the body. The lower sign P indicates the quantity of the linear system. $K_{W(B)P}$ and $K_{B(W)P}$ are identical [1].

Based on the "leading edge suction analogy" theory, the normal lift of a single wing is equal to [5]

$$C_{N_W} = C^{\alpha}_{N_W} \sin\alpha\cos\alpha + (\tilde{K}_{VLE} + \tilde{K}_{VSE})\sin^2\alpha \qquad (2)$$

$$\tilde{K}_{VLE} = C^{\alpha}_{N_W}\left(1 - \frac{C^{\alpha}_{N_W}}{\pi A}\right) / \cos\Lambda$$

$$\tilde{K}_{VSE} = 2\left(\frac{c_s}{s_m}\right)\frac{(C^{\alpha}_{N_W})^2}{\pi A}.$$

In the formula, $\tilde{K}_{VLE}$ and $\tilde{K}_{VSE}$ are separately the leading edge vortex and side edge vortex lift derivatives. If we assume that the "suction analogy" theory is also applicable to the wing-body combination, then at this time it is necessary to come forth with more non-linear interference factors

$$C_{N_{(B+WB)}} = C_{N_B} + \{(K_{W(B)P} + K_{B(W)P})C^{\alpha}_{N_W}\sin\alpha\cos\alpha + (K_{W(B),VLE} + K_{B(W),VLE})\tilde{K}_{VLE}\sin^2\alpha + (K_{W(B),VSE} + K_{B(W),VSE})\tilde{K}_{VSE}\sin^2\alpha\} \frac{S_W}{S_B} \qquad (3)$$

In this formula, the definitions of each non-linear interference

factor are separately

$$K_{W(B),VLE} = \frac{C_{N_{W(B),VLE}}}{C_{N_{VLE}}}, \quad K_{B(W),VLE} = \frac{C_{N_{B(W),VLE}}}{C_{N_{VLE}}},$$
$$K_{W(B),VSE} = \frac{C_{N_{W(B),VSE}}}{C_{N_{VSE}}}, \quad K_{B(W),VSE} = \frac{C_{N_{B(W),VSE}}}{C_{N_{VSE}}}.$$

The lower signs VLE and VSE separately indicate the quantity caused by the wing's leading edge vortex and side edge vortex. If the normal force distribution $c(\eta)c_{nv}(\eta)$ produced along the spanwise direction vortex is known, then

$$C_{N_{W(B),VLE}} = \frac{2}{S_W}\int_r^1 c(\eta)c_{nv}(\eta)d\eta. \qquad (4)$$

$\eta = \frac{y}{s_m}$ and $\xi = \frac{x}{c_r}$ are separately the spanwise and chordwise dimensionless distances,

$$\bar{r} = \frac{r}{s_m}, \quad \bar{c}(\eta) = \frac{c(y)}{c_r}, \quad \bar{S}_W = \frac{S_W}{s_m c_r}$$

are separately the dimensionless radius chord length and wing area (below we will omit all of the "-" signs). See fig. 1.

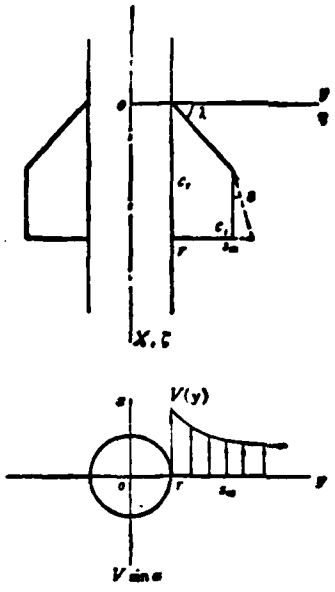

Fig. 1 Diagram of Geometric Measurements

Reference [5] pointed out that the long and thin triangular wing can approximately take the vortex produced normal force as a linear distribution. Because this article is mainly concerned with the wing-body combination interference factors, if we take the leading edge vortex produced normal force for most of the wing surfaces as having linear distribution, then

$$c(\eta)c_{n_v}(\eta) = \pi(\eta - r)\sin^2\alpha_\eta / \cos\Lambda. \quad (5)$$

$(\eta-r)$ is the spanwise distance starting from the outer exposure of the wing root chord. a_η is the local attack angle because at this time the wing is located in the upwash flow field caused by the body. If we consider that the length of the body is sufficient and overlook the nose effect, then the local attack angle distribution on the symmetrically level surface in the cross flow plane is

$$\sin\alpha_\eta = \left(1+\frac{r^2}{\eta^2}\right)\sin\alpha_\infty \qquad (6)$$

After substituting formulas (5) and (6) into formula (4), we can obtain

$$K_{W(B),VLE} = \frac{2r^2}{(1-r)^2}\left\{\frac{1}{3}r^3 - \frac{1}{2}r^2 + 2r - \frac{4}{3} - \frac{1}{r} + \frac{1}{2r^2} - 2\ln r\right\} \qquad (7)$$

The kinematic conditions on the body surface should be sufficient, that is, the surface should be a stream line. For this reason, we should place a corresponding vortex image system on the body. Therefore, the added normal power of the vortex produced normal force derived on the body is

$$C_{N_{B(W)},VLE} = \frac{2}{S_W}\int_{r^2}^{r} c(\eta_1)c_{nv}(\eta_1)d\eta_1$$

Because $d\eta_1 = -\frac{r^2}{\eta^2}d\eta$, $c(\eta_1)c_{nv}(\eta_1)=c(\eta)c_{nv}(\eta)$, therefore

$$C_{N_{B(W)},VLE} = \frac{2\pi}{S_W}\int_r^1 (\eta - r)\left(1+\frac{r^2}{\eta^2}\right)^2\frac{r^2}{\eta^2}d\eta$$

After operation we obtain

$$K_{B(W),VLE} = \frac{2r^2}{(1-r)^2}\left\{r - r^2 + \frac{2}{3}r^3 - \frac{1}{4}r^4 + \frac{1}{5}r^5 - \ln r - \frac{37}{60}\right\} \qquad (8)$$

Based on the method found in reference [5], the side edge

outside partial ε angle is transformed into a part of the leading edge and when ε tends towards zero, we can compute the side edge vortex produced normal force.

$$C_{N_{W(B),VSE}} = \frac{2\pi}{S_W} \lim_{\varepsilon \to 0} \left\{ \int_1^{1+\varepsilon_{\eta^4}} (\eta - r)\left(1 + \frac{r^2}{\eta^2}\right)^2 \Big/ \operatorname{tg} \varepsilon \, d\eta \right\}$$

$$C_{N_{B(W),VSE}} = \frac{2\pi}{S_W} \lim_{\varepsilon \to 0} \left\{ \int_1^{1+\varepsilon_{\eta^4}} (\eta - r)\left(1 + \frac{r^2}{\eta^2}\right)^2 \frac{r^2}{\eta^2} \Big/ \operatorname{tg} \varepsilon \, d\eta \right\}$$

Therefore

$$K_{W(B),VSE} = (1 + r^2)^2 \tag{9}$$

$$K_{B(W),VSE} = r^2(1 + r^2)^2 \tag{10}$$

In the same way, we can find the corresponding center of pressure position

$$\bar{\xi}_{W(B),VLE} = \frac{2\pi \tan \Lambda}{S_W C_{N_{W(B),VLE}}} \int_r^1 (\eta - r)^2 \left(1 + \frac{r^2}{\eta^2}\right)^2 d\eta$$

$$\bar{\xi}_{B(W),VLE} = \frac{2\pi \tan \Lambda}{S_W C_{N_{B(W),VLE}}} \int_r^1 (\eta - r)^2 \left(1 + \frac{r^2}{\eta^2}\right)^2 \frac{r^2}{\eta^2} d\eta$$

Therefore

$$\bar{\xi}_{W(B),VLE} = \frac{1}{K_{W(B),VLE}} \frac{2r^2}{(1-r)^3} \left\{ \frac{1}{3} - r + 3r^2 - 3r^4 + r^5 - \frac{1}{3} r^6 + 4r^3 \ln r \right\} \tag{11}$$

$$\bar{\xi}_{B(W),VLE} = \frac{1}{K_{B(W),VLE}} \frac{2r^2}{(1-r)^3} \left\{ 1 + \frac{7}{10} r - 3r^2 + 2r^3 - r^4 + \frac{1}{2} r^5 - \frac{1}{5} r^6 + 2r \ln r \right\} \tag{12}$$

As for $x'_{W(B),VSE}/c_t$ and $x'_{B(W),VSE}/c_t$, we can in the same way find

$$\frac{x'_{W(B),VSE}}{c_t} = \frac{x'_{B(W),VSE}}{c_t} = \frac{1}{2} \qquad (13)$$

In the formula, x' is the chordwise distance beginning from the side edge apex quantity.

(7)-(10) are then four non-linear interference factors and (11)-(13) are their corresponding center of pressure positions. Figs. 2-4 show their changes with $(\frac{r}{s_m})$ and from the figures we can see that the changes of the non-linear interference factors tend to be basically the same as the linear interference factors $K_{W(B)P}$ and $K_{B(W)P}$. When $\frac{r}{s_m} \longrightarrow 0$, $K_{W(B),VLE}$ and $K_{B(W),VSE} \longrightarrow 1$, and $K_{B(W)VLE}$ and $K_{B(W)VSE} \longrightarrow 0$; when $\frac{r}{s_m} \longrightarrow 1$, they all tend towards 4. Fig. 3 is the relative shift of the wing's leading edge vortex produced normal force center of pressure. If the vortex produced normal force center of pressure of a single wing can be directly derived, then we can raise the precision of $x_{W(B)VLE/c_r}$.

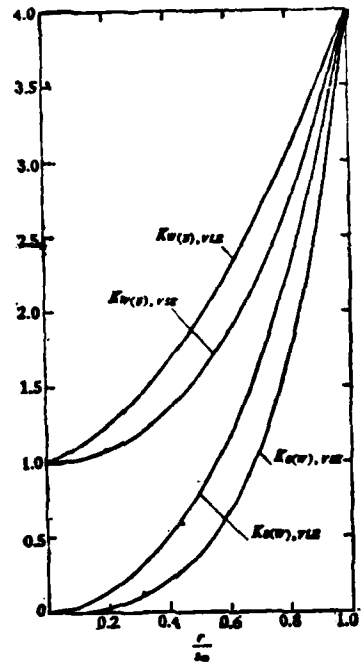

Fig. 2 The Non-Linear Interference Factors of Wing-Body Combinations

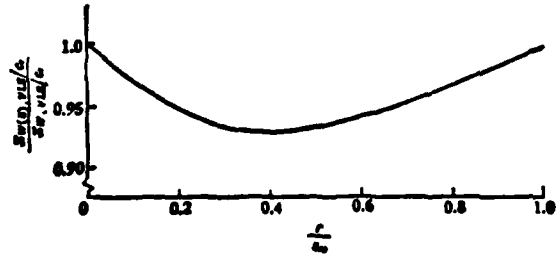

Fig. 3 The Relative Shift of the Wing's Leading Edge Vortex Produced Normal Force Center of Pressure When There is a Body

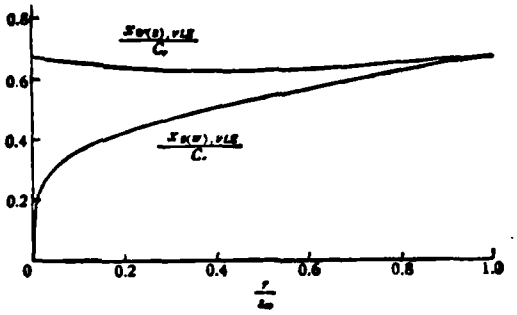

Fig. 4 The Wing's Leading Edge Vortex Produced Normal Force Center of Pressure $\frac{x_{W(B),VLE}}{c_r}$ and the Normal Force Center of Pressure $\frac{x_{B(W),VLE}}{c_r}$ of the Leading Edge Vortex Derived on the Body When There is a Body

2. Computation Examples and Discussion

To test and verify the accuracy of the results obtained in this article, we carried out calculations on the data presented in reference [6] and also made a comparison with the calculation method of reference [6] (fig. 5).

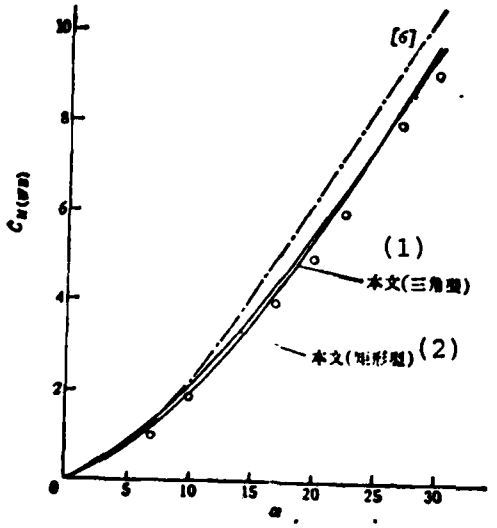

Fig. 5(a) Normal Force of Wing-Body Combination

⊙ Rectangular wing and triangualr wing tests [6] of $\frac{L}{D}=12$

Key: 1. This article (triangular type)
2. This article (rectangular type)

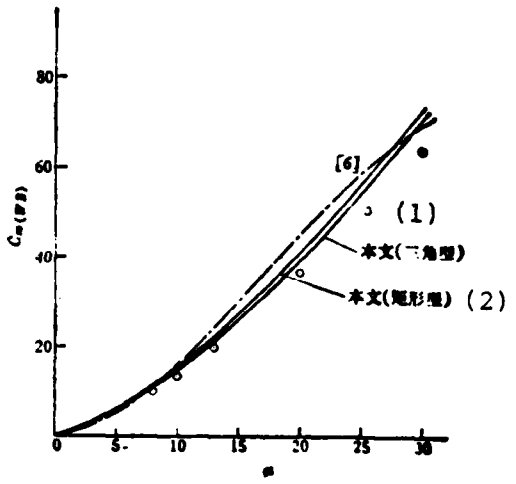

Fig. 5(b) Pitching Moment of Wing-Body Combination

⊙ Rectangular wing and triangular wing tests [6] of $\frac{L}{D}=12.0$

Key: 1. This article (rectangular type)
2. This article (triangular type)

Reference [6] considers that an equivalent rectangular substitution can be used for all wing surfaces and it is only necessary that $\frac{r}{s_m}$ are all identical. When the surface area and center of surface position are identical, then there are identical normal force and moment. His own test data reveals this point and the two calculated curves of the rectangular wing and triangular wing given in this article are very close to it. This also confirms that the non-linear interference factors in this

article can be used.

The range applied in this article is the same as that of the "suction analogy" theory. When the attack angle is very large, the leading edge vortex can "split" on the wing surface. At this time, the "suction analogy" cannot be used. This is especially the case under transonic and supersonic speeds when the large attack angle flow field is very complex. Reference [7] points out that at this time the interference factor is the derivative of the attack angle and Mach number. At present, there is still no successful theoretical method which can sufficiently solve this problem. Aside from this, in this article we did not consider the downwash effect of the nose vortex on the wing surface.

References

[1] Pitts, W.C., Nielsen, J.N., Kattar, G.E., NACA Rep. 1307(1957).

[2] Lebedev, et. al., Flight dynamics of Unmanned Aircraft, National Defense Publishing House(1964).

[3] Ji Chuchun, et. al., Aerodynamic computation handbook for winged aircraft, National Defense Publishing House(1979).

[4] Nielsen, J.N., et.al., NASA CR-2473(1975)

[5] Yin Xieyuan, Aviation, 1, 1(1980), 1-6.

[6] Thomson, K.D., Aeronautical Quarterly, XXVIII part 3(1976.3).

[7] Nielsen, J.N., AIAA paper, 78—20.

Abstract

Based upon leading edge-suction analogy and upwash theory and following the concept of interference factors proposed by J. N. Nielson, a method for predicting the interference factors of vortex-lift due to separation flow along leading (or side) edges of wing-body combination at subsonic speed is presented.

Related formulas and curves are obtained. They have wider range of applicability than those available in current handbooks.